COUPLED SURFACE PLASMON STRUCTURES AND APPLICATIONS

A THESIS

SUBMITTED TO THE DEPARTMENT OF MATERIALS SCIENCE AND NANOTECHNOLOGY

AND THE INSTITUTE OF ENGINEERING AND SCIENCES

OF BILKENT UNIVERSITY

IN PARTIAL FULFILLMENT OF THE REQUIREMENTS

FOR THE DEGREE OF

MASTER OF SCIENCE

By

Kemal Gürel

September 2009

I certify that I have read this thesis and that in my opinion it is fully adequate, in scope and in quality, as a thesis for the degree of Master of Science.

Assist. Prof. Dr. Mehmet Bayındır (Supervisor)

I certify that I have read this thesis and that in my opinion it is fully adequate, in scope and in quality, as a thesis for the degree of Master of Science.

Res. Assist. Prof. Dr. Aykutlu Dana (Co-Supervisor)

I certify that I have read this thesis and that in my opinion it is fully adequate, in scope and in quality, as a thesis for the degree of Master of Science.

Assoc. Prof. Dr. Mehmet Özgür Oktel

I certify that I have read this thesis and that in my opinion it is fully adequate, in scope and in quality, as a thesis for the degree of Master of Science.

Assist. Prof. Dr. Ali Kemal Okyay

Approved for the Institute of Engineering and Sciences:

Prof. Dr. Mehmet Baray
Director of Institute of Engineering and Sciences

ABSTRACT

COUPLED SURFACE PLASMON STRUCTURES AND APPLICATIONS

Kemal Gürel
M.S. in Materials Science and Nanotechnology
Supervisor: Assist. Prof. Dr. Mehmet Bayındır
September 2009

Surface plasmons have attracted great interest during past decades due to their unique physical properties. In this thesis, we study grating-coupled surface plasmons for sensing and filtering applications. We first present simple physical and chemical procedures that allow tuning and modification of the topography of gratings present in optical storage discs into geometries optimal for grating coupled plasmon resonance excitation. After proper metal coating, the tuned surfaces exhibit sharp plasmon resonances that can be excited at wavelengths ranging from 260 nm to over 2.7 μm with relatively high quality factors. As an immediate exemplary application, use of such optimized gratings in aqueous medium for refractive index measurement is demonstrated.

We also report another plasmonic component based on a pair of surfaces displaying grating coupled plasmon enhanced transmission. We observe high quality factor transmission peaks as high as 100 through our plasmonic filter based on gratings obtained directly from optical storage disks. Wavelength and polarization dependent transmission is also demonstrated in the visible and infrared portions of the spectrum. The resonance wavelength of this filter can be tuned by simply changing the angle of incidence. Numerical calculations agree well

with measurements. Our work can open up directions toward disposable optical components such as filters and polarizers.

Morever, we investigate plasmonic force between two coupled metallic layers. We observe the mode splitting due to coupling between plasmonic surfaces by using finite difference time domain simulations.

Keywords: Surface Plasmons, Grating Coupling, Optical Disks, Filter, Prism Coupling, MIM Waveguide, Mode Splitting, Plasmonic Force.

ÖZET

ÇİFTLENMİŞ YÜZEY PLAZMON YAPILARI VE UYGULAMALARI

Kemal Gürel
Malzeme Bilimi ve Nanoteknoloji Yüksek Lisans
Tez Yöneticisi: Yar. Doç. Dr. Mehmet Bayındır
Eylül 2009

Yüzey plazmon yapıları kendilerine has karakteristik özelliklerinden ötürü son yıllarda fizik ve mühendislik dalında her gün daha fazla ilgi toplayan bir konu oldu. Bu tezde biz, öncelikle ızgaralı kuplaj metoduyla yüzey plazmonlarının uyarılması, bu plazmon yapılarının da sensör ve filtre uygulamaları olarak kullanılışı üzerine yaptığımız çalışmaları sununuyoruz. Izgaralı kuplaj metodunda başlangıç malzemeleri olarak optik diskleri kullandık. Bu disklerin yüzey yapılarını basit fiziksel ve kimyasal metodlarla modifiye ettik. Sonrasında bu yüzeylere yeterli miktarda metal kaplamak suretiyle keskin rezonans figürleri elde ettik. Izgaralı kuplaj yönteminde spektrum hem ızgara periyoduna hem de elektromanyetik dalganın geliş açısına bağlı olduğu için dalgaboyu olarak 260 nm'den 2.7 μm'ye kadar uzanan geniş bir yelpazede çeşitli rezonanslar yakalayabildik. Hemen akla gelebilecek bir uygulama olarak da ürettiğimiz bu yapıları sulu ortamda kırılma indisi ölçümü uygulamalarında kullandık.

Ayrıca, bu tezde optik diskleri kullanarak yaptığımız yüzey plazmon uyarımı üzerine çalışan bir geçirim filtresi de gösteriyoruz. Bu filtreden aldığımız ölçümlerde oldukça keskin geçirim spektrumları elde ettik, öyle ki 100'e kadar varan kalite faktörlerine ulaşabildik. Böylece dalgaboyu ve polarizasyona bağlı

olarak değişkenlik göstererek çalışan bir optik filtre uygulamasını ortaya koymuş olduk. Bu geçirim spektrumumuz görünür dalgaboylarından yakın kızılötesi dalgaboylarına kadar uzanmaktadır. İstediğimiz dalgaboyunu geliş açısını değiştirerek ayarlayabiliriz. Nümerik hesaplarımız da yaptığımız ölçümlerimizle gayet uyumlu sonuçlar vermektedir. Bu çalışmamızın ileride kullan-at tarzında filtre ya da polarizör benzeri optik öğeler olabileceğini göstermesi açısından önem arz ettiğini düsünüyoruz.

Asıl iş olarak ızgaralı plazmon yapılar üzerine çalışmamıza rağmen, bir yandan da prizmalı kuplaj metodundan başlayarak metal yalıtkan metal (MYM) dalgakılavuzu yapılarının elektromanyetik olarak incelenmesi üzerine minör çalışmalar yaptık. Bu çalışmalarımızda iki metalli plazmonik sistemlerin spektrum olarak tek metalli normal sistemlerden farkını inceledik ve sonuç olarak spektrumda ciddi bir ayrışma gözlemledik. Bu ayrışma sonucu oluşan farklı modların da farklı elektrik alan dağılımlarını yansıttığını FDTD metoduyla gösterdik. Bu dağılımlara dayanarak da metal yüzeyler arasında bir plazmonik kuvvet öngördük.

Anahtar Kelimeler: Yüzey Plazmonları, Izgaralı Kuplaj, Optik Diskler, Filtre, Prizmalı Kuplaj, MYM Dalgakılavuzu, Mod Ayrışımı, Plazmonik Kuvvet.

ACKNOWLEDGMENTS

First of all I would like to thank to my thesis advisors Prof. Mehmet Bayındır and Prof. Aykutlu Dana for their invaluable guidance, one-to-one special working environment, encouragement and help during my master study in Bilkent. I would like to thank to my jury members Prof. Mehmet Özgür Oktel and Prof. Ali Kemal Okyay as well, for evaluating my thesis. I would also like to thank to Prof. Salim Çıracı due to his efforts for establishment of UNAM.

I secondarily want to thank to my colleagues Özlem Şenlik, Burkan Kaplan and Hasan Güner for their patience, help and sacrifices they have made while working with me. I would also like to thank to my dearest friends and group members Adem Yildirim, Özlem Şenlik, Yavuz Nuri Ertaş, H. Esat Kondakçı, Özlem Köylü, Hülya Budunoğlu, Erol Özgür, Ekin Özgür, Duygu Akbulut, Dr. Hakan Deniz, Dr. Abdullah Tülek, Can Koral and Ahmet Ünal for any kind of help, chat, food, friendship and sharing during the two years I spent at UNAM.

I would like to thank to TÜBİTAK for their financial support through 2228 coded scholarship and UNAM for giving me a research assistant scholarship.

I want to thank to Dr. Mecit Yaman in special for sharing his scientific vision, cultural knowledge, life experiences, futuristic thoughts and *The Economist* journal with me. Finally, I send most special appreciations to Murat Kılınç and Mert Vural, who have been my brothers rather than friends in my Bilkent life.

Contents

List of Figures

Dedicated to

my little brother

Ege Gürel

Chapter 1

MOTIVATION

Optics, with its numerous vital technological applications in industry, is an inevitably integrated part of our daily life. Its evolution started with people's usage of light for specific purposes that are parallel to their needs in life. First optical components that are worth mentioning are mirrors made by ancient Egyptians using polished metals about 1900 BC [1]. Nowadays, optics is everywhere we see. Any kind of imaging equipment, each movie we watch, most sensitive measurement equipments and the speed of Internet are products of today's optics technology.

Quite possibly, preliminary improvements at optics technology were achieved by trial and error method. First theories about the nature of light were put forward by the Greek scientist/philosopher Euclid in 4th century BC. Originating from his geometry knowledge he came up with several self-evident axioms explaining some properties, including reflection of light. After Euclid, until the time of Al-Hazen (965-1040 AD), we see two more important people, who contributed significantly to the field of optics. Hero of Alexandria claimed that light propagates at infinite speed and it follows the shortest path between two points. He also derived the law of reflection, firstly proposed by Euclid, using

this shortest path approach. About 150 years later Cladius Ptolemy stated a primitive version of law of refraction, which works fine only for incidence angles close to normal. Despite its inaccuracy for large incidence angles this formulation stayed valid for about 1500 years, until Willebrord Snell (1580-1626) corrected it in 1621. By many authorities Al-Hazen, also known as father of modern optics, is considered the first person who studied optics according to scientific methods. He showed that light rays propagate in straight lines. Using lenses and mirrors he experimentally investigated refraction and reflection phenomena. He also reduced light rays into vertical and horizontal components, and obtained results similar to Snell's law. Following Al-Hazen's initiative works, Roger Bacon (1214-1294) described the magnification effect of convex lenses and used these lenses for correcting eyesight. In 17^{th} century Hans Lippershey, Galileo Galilei and Johannes Kepler used lenses to build telescopes, Zacharias Janssen and Francisco Fontana for inventing the microscope. After Willebrord Snell formulated the correct law of refraction at 1609, this media dependent behavior of light has opened the door to modern applied optics. Until the end of 17^{th} century common belief was that light propagates as ray in nature and that is why research on optics was concentrated on geometric optics. Robert Hooke (1635-1703) was first to study the colored interference pattern of light and can be count as the initiator of wave theory. Later Christiaan Huygens (1629-1695), Thomas Young (1773-1829) and Augustine Jean Fresnel (1788-1827) extended wave theory. Finally, James Clark Maxwell (1831-1879), by summarizing and integrating all electromagnetic knowledge that exists at that time, formulated his brilliant equations and today we still use basically these equations to explain the behavior of light.

For hundreds of years people studied light propagating in dielectric materials, because metals are lossy at optical wavelengths and skin depth of light was not higher than a few tens of nanometers in these materials [2]. They were generally used as reflectors to manipulate the travelled path of light. Interesting case about metals is their free electrons, which have their own oscillation frequency.

In 20^{th} century researchers pointed out that if the appropriate conditions were satisfied, optical signals have the ability to generate resonant oscillations in metals, such as gold and silver. This phenomenon is named as plasmon resonance by scientific authorities and has become a very popular research topic for recent decades. First time observation of surface plasmons was reported by Wood [3] in 1902. He reported that when a metal diffraction grating is illuminated with polychromatic light, dark narrow bands are observed in the spectrum of diffracted light. He named these dark bands, which actually correspond to surface plasmon resonance excitations, as anomalies. His work was mainly experimental. Theoretical work about this anomaly concept is first concluded by Fano [4]. He proposed that these anomalies are results of evanescent electromagnetic waves excited at the surface of diffraction grating. In 1958 Thurbadar set up an experiment and measured reflection of light from thin metal films on substrates [5]. He observed high drops in reflectivity, but he did not relate this to surface plasmons. Otto worked on Thurbadar's results and explained that this drop at the attenuated total reflection is due to the excitation of surface plasmons [6]. Just after Otto's formulation, in the same year Kretschmann and Raether modified the Attenuated Total Reflection configuration a little and proposed the surface plasmon resonance system which is the most common commercially available surface plasmon sensor today [7]. Following the pioneering works in 1960s people used surface plasmons for thin metal film characterization, metal boundary electromagnetic problems, waveguide and sensor applications.

Surface plasmon applications generally draw attention of the researchers due to three main reasons. First and most important one is subwavelength applications of plasmonics [8]. Since surface plasmon oscillations originate from coupling between electron plasma oscillations and optical waves, wavelength of plasmons is generally less than the coupling wavelength. This feature is quite useful for especially electronics industry [9]. People in electronics industry always desired to integrate optics into electronics due to speed issues at the chips. However,

fabrication technology in electronics has the capability for mass production of 45 nm gate transistors today. With conventional methods it is impossible to beat the diffraction limit of light at devices [10]. For that reason most of the electro-optic researchers directed their path to the plasmonics topic. Secondary reasons for that much popularity are high intensity of the evanescent waves at the metal dielectric boundaries and high quality factors achieved at the plasmon resonance condition. High intensity at the surface opens way to nonlinear applications of surface plasmons [11, 12]. On the other hand, sharp resonance condition lets us to fabricate high sensitivity sensors which are generally used for biological or chemical sensing [13, 14]. These sensors generally work with measurement of refractive index change principle and the cutting edge ones have very high and accurate sensitivities less than $1x10^{-5}$ relative index unit (RIU) [14].

Except these main applications surface plasmon waves are also used in transmission and waveguiding applications. Since the pioneering work of Ebbessen [15] plasmons are used for transmission of light through optically thick metal films. Transmission property was demonstrated with several geometries. From the scientific point of view beating the skin depth was quite new and interesting. From engineering perspective however, a new polarization dependent optical filter concept was demonstrated. Waveguiding is also very important from the engineering perspective. With this property, light could be bent and lead through subwavelength structures in integrated circuits. Also the investigation of layered structured waveguides Metal-Insulator-Metal (MIM), Insulator-Metal-Insulator (IMI) etc. for plasmonic applications has been an interesting topic for recent decades' optics research [16, 17, 18].

Plasmonics has entered the scientific world gradually. However, starting from 1980s people who work on surface plasmons' fundamentals and applications grew like an avalanche. It is a still growing subject and there is a lot to do in this

topic. All these motivated us that plasmonics and its applications is a subject worth to get a master's degree on.

In this thesis, we study Surface Plasmon Resonance (SPR) nanostructures and their applications. Our work consists of two main subjects, SPR on optical storage disks and plasmonic force investigation at MIM waveguide structures. Former one includes modification and usage of optical storage disks (CD, DVD, Blu-Ray) as compact SPR devices, obtaining polarization and incidence angle dependent optical filters with this structures. This work is realized experimentally and it is supported with numerical simulations [19, 20]. On the other hand MIM waveguide investigation for plasmonic force part of the subject could not be performed experimentally. However, numerical simulations agree well with our predictions.

SPR structures constitute a quite large research area for both engineers and physicists. However, because of the nanostructured sizes it is hard to fabricate and deal with these structures. In the beginning we defined our problem as beating this difficulties and aimed to achieve a compact and user friendly work environment for plasmonics. For that purpose we started to use corrugations that already exist on optical storage disks. Later on, after optimization of this procedure we wanted to see these devices in action. So, we designed a filter from these structures and realized it as an optical device. At the MIM waveguide case we wanted to see the effect of the interaction between the metals when we perturb a Metal Insulator (MI) surface plasmon waveguide by bringing one more metal closer to the system.

Our contributions can be summarized as follows:

- We proposed a new technique for usage of optical disks in plasmonics research. We showed the importance of grating modification and how to controllably modify the gratings by etching. Also due to different periods

of optical disks we could achieve plasmon resonances ranging from UV to NIR. A final remark about disk modification is this modification procedure let us increase the quality factor of achieved resonances.

- Originating from the resonance phenomenon we prospected that thin silver films could let the light pass through at resonance condition. We examined this hypothesis by using pre-modified optical disks. We fabricated a device, with optimum gratings at both sides which are metal-coated. So we obtained an optical filter, the spectrum of which is wavelength, polarization and incident angle dependent.

- In addition to the works mentioned above, we examined the perturbation at single metal insulator waveguide. We expected to observe the splitting phenomenon around the resonance wavelength which is determined at the single metal case. This splitting would represent the bonding and anti-bonding modes of the system. So we expected to observe different field profiles at these separate modes. Investigation of these modes is an important research topic by itself because symmetric and anti-symmetric field distributions suggest an excited force between metals, which we will name plasmonic force.

In Chapter 2, we first provide the basic theoretical background that is necessary for study of plasmonics. Starting from Maxwell's equations we will show the surface plasmon resonance wave solutions and state the conditions needed for this resonance. In Chapter 3 we will show how we dealed with optical storage disks and converted them into compact SPR devices. Chapter 4 addresses the coupled system that we encounter at the MIM waveguide case. Interaction's effect onto the spectrum is analyzed and the resulting force is suggested. Finally, we conclude our work and list some future prospects about this research area in the Chapter 5.

Chapter 2

THEORETICAL BACKGROUND

2.1 Surface Plasmons

Surface plasmons are the evanescent electromagnetic waves that are results of interaction processes between electromagnetic radiation and conduction electrons at metal-insulator interfaces. In this section we will give the basic theoretical knowledge necessary for studying behaviors of these waves. For that purpose, we will investigate the electromagnetic behavior of metals at optical wavelengths. Starting from free electron gas model we will derive dielectric functions of metals. Then we will show the solutions of Maxwell's equations for surface plasmons at metal insulator interfaces. We will examine the necessary conditions about material selection, polarization of incoming light, momentum matching etc. necessary for achieving the plasmon resonance. Finally, we will describe the methods used to excite surface plasmons in detail.

2.1.1 Dielectric Function of Metals

For optics research, metals have mostly been not that interesting. It is a common fact that metals do not let optical waves pass through. Moreover, they reflect most of incident wave at a large spectrum ranging from microwave up to visible wavelengths. For these reasons, people generally used metals as cladding to prevent escape of light from the system. For low frequency regime, metals act like perfect or good conductors. When low frequency EM waves hit onto metals they reflect back with little amounts of penetration depths and negligibly minor loss of energy. In the visible part of the spectrum this penetration increases and leads to more loss. As we approach the UV part of the spectrum, metals converge to dielectrics and become transparent after a certain frequency threshold. This highly dispersive behavior leads us to generate a dispersion model for metals. So we need an $\epsilon(\omega)$ formulation.

Optical properties of metals are generally modelled by plasma model. Plasma does not deal with details of lattice potential and electron-electron interactions. Instead, it considers that band structure properties are based on the effective optical mass m of each electron. When electromagnetic waves penetrate into the metal they oscillate free electrons. However, their oscillations damp due to collisions occurring with a collision frequency $\gamma = 1/\tau$. τ is named as the relaxation time of free electron gas and at room temperature it is on the order of 10 fs which corresponds to 10^{14} collisions at a second.

At the plasma model, motion equation of an electron with respect to an applied electric field $\mathbf{E}$

$$m\ddot{\mathbf{x}} + m\gamma\dot{\mathbf{x}} = -e\mathbf{E}, \tag{2.1}$$

Due to its harmonic time dependence, applied electromagnetic wave is in the form $\mathbf{E}(t) = \mathbf{E}_0 \mathrm{e}^{-i\omega t}$. So we expect the solution of the differential equation to

be in the form of $\mathbf{x}(t) = \mathbf{x}_0 e^{-i\omega t}$ as well. The particular solution of this equation brings

$$\mathbf{x}(t) = \frac{e}{m(\omega^2 + i\gamma\omega)}\mathbf{E}(t), \tag{2.2}$$

Displacement of these electrons by applied EM wave causes macroscopic polarization in the metal which is formulated as $\mathbf{P} = -ne\mathbf{x}$ i.e.

$$\mathbf{P} = -\frac{ne^2}{m(\omega^2 + i\gamma\omega)}\mathbf{E}, \tag{2.3}$$

Also as a result of Maxwell's equations we know that $\mathbf{D} = \epsilon_0\mathbf{E} + \mathbf{P}$. Putting this result in our equation we obtain

$$\mathbf{D} = \epsilon_0 \left(1 - \frac{{\omega_p}^2}{\omega^2 + i\gamma\omega}\right)\mathbf{E}, \tag{2.4}$$

where we named ${\omega_p}^2 = \frac{ne^2}{\epsilon_0 m}$ as the square of plasma frequency of free electron gas. After all we get the equation we desired for dielectric function of metals

$$\epsilon(\omega) = 1 - \frac{{\omega_p}^2}{\omega^2 + i\gamma\omega}. \tag{2.5}$$

Say $\epsilon(\omega) = \epsilon_1(\omega) + i\epsilon_2(\omega)$, then real and imaginary parts of $\epsilon(\omega)$ are

$$\epsilon_1(\omega) = 1 - \frac{{\omega_p}^2\tau^2}{1 + \omega^2\tau^2}, \tag{2.6}$$

$$\epsilon_2(\omega) = \frac{{\omega_p}^2\tau}{\omega(1 + \omega^2\tau^2)}. \tag{2.7}$$

When we work at frequencies close to ω_p, $\omega\tau >> 1$. Imaginary part of the dielectric constant vanishes and Equation 2.5 converges to

$$\epsilon(\omega) = 1 - \frac{{\omega_p}^2}{\omega^2}. \tag{2.8}$$

However, for surface plasmon applications we stay at frequencies smaller than plasma frequency and use Equation 2.5. This model is known as Drude model [21] for dielectric function of metals and it is the most common mathematical model used for characterization of metals at numerical tools. The constants ω_p and γ are determined with respect to the model fitted onto the actual dielectric constant data [22]. A fitted data for gold and silver is given at Figure 2.1 [23] .

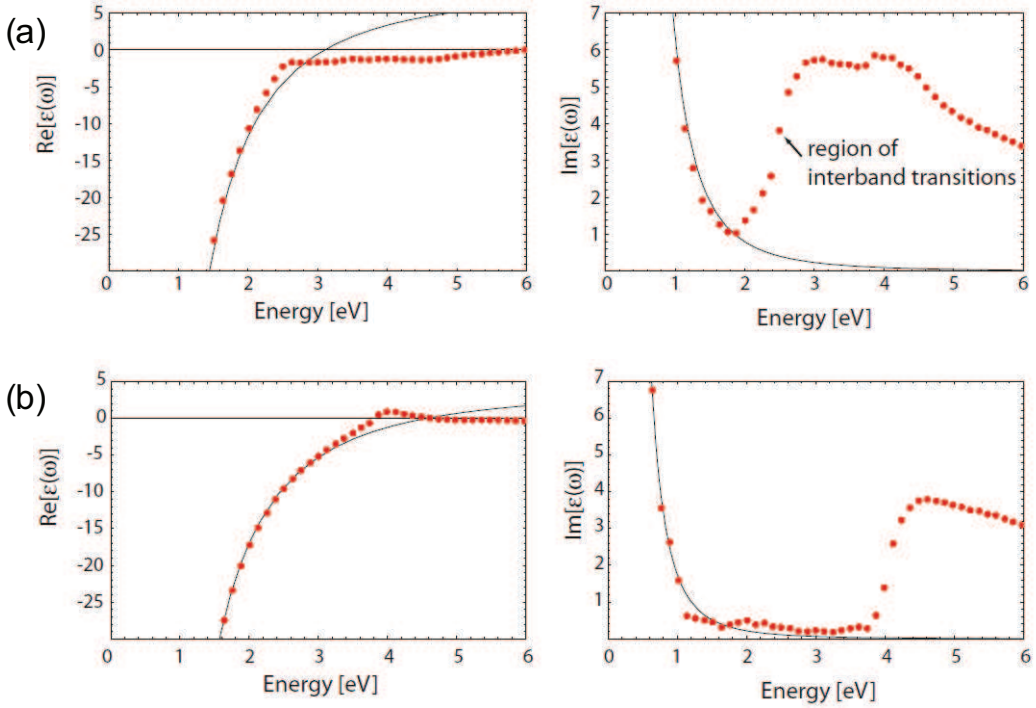

Figure 2.1: Dielectric constants of metals Au **(a)** and Ag **(b)** with respect to photon energy. Dotted lines are actual data by Cristy, fitted lines are Drude models for these metals.

2.1.2 Suface Plasmons at Metal Dielectric Boundaries

As is well known, metal dielectric interfaces are able to sustain surface plasmon polaritons. Coherent longitudinal charge oscillations of conduction electrons of metal allows the propagation of the surface plasmons at the interface (Fig. 2.4). The field distribution caused due to these oscillations has its maximum at the boundary and its amplitude decays proportional with its distance to the boundary.

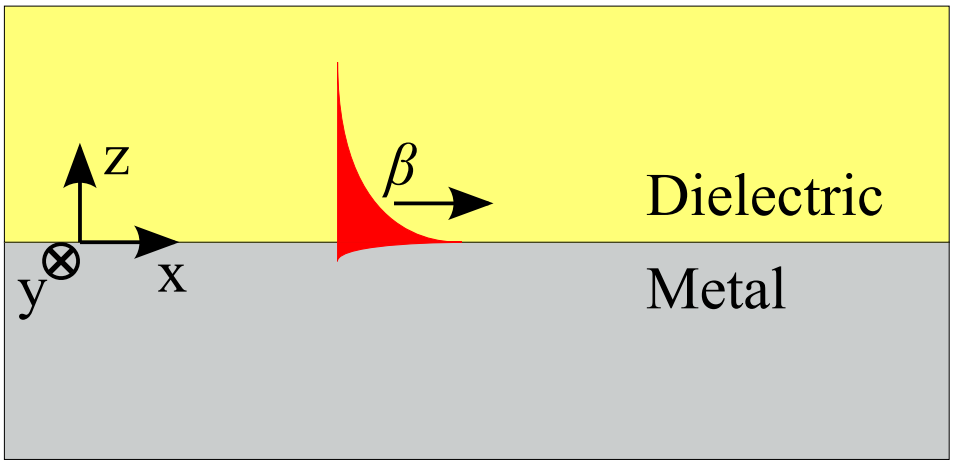

Figure 2.2: Intensity and propagation schematic of a surface plasmon wave at a metal-dielectric interface. The intensity decays exponentially with a maximum at the interface. Predictably, intensity drop in the metal is much faster than the drop in the dielectric. Also the propagation of the surface plasmon is parallel to the interface.

The field distribution caused by surface plasmons is also explained by solution of Maxwell's equations. A convenient starting point would be the fundamental equation of electromagnetic wave theory. When we work at a nonmagnetic media and if ϵ does not differ significantly with distance, we get the wave equation

$$\nabla^2\mathbf{E} - \frac{\epsilon}{c^2}\frac{\partial^2\mathbf{E}}{\partial t^2} = 0. \tag{2.9}$$

Due to the harmonic time dependence of electromagnetic waves we know that $\mathbf{E}(t) = \mathbf{E}\mathrm{e}^{-iwt}$, and putting this model into Equation 2.9 we obtain

$$\nabla^2\mathbf{E} + k_0^2\epsilon\mathbf{E} = 0. \tag{2.10}$$

With respect to Figure 2.4 propagating surface plasmon waves can be formulated as $\mathbf{E}(z)\mathrm{e}^{i\beta x}$. Here $\beta = k_{sp}$ is the propagation constant of the surface plasmon, which propagates along x axis. Putting this last expression into Equation 2.10 we get

$$\frac{\partial^2 \mathbf{E}(z)}{\partial z^2} + (k_0^2\epsilon - \beta^2)\mathbf{E} = 0. \tag{2.11}$$

Now we have the wave equation that should be satisfied. Note that this equation also holds for **H** field. However, we still do not have an explicit formulation of the different field components of the electromagnetic wave. This expression for surface plasmon waves can be achieved using Maxwell's Curl Equations.

$$\nabla \times \mathbf{E} = -\frac{\partial \mathbf{B}}{\partial t}, \tag{2.12}$$

$$\nabla \times \mathbf{H} = \mathbf{J_{ext}}\frac{\partial \mathbf{B}}{\partial t}. \tag{2.13}$$

We assume that there is no surface current excited due to the electromagnetic field's interaction with materials. The operator $\frac{\partial}{\partial t}$ is equal to multiplication with $-i\omega$, and we have $\frac{\partial}{\partial y} = 0$ due to the homogeneity along y-axis. Finally, since our field is in the form $\mathbf{E}(z)\mathrm{e}^{i\beta x}$ the operator $\frac{\partial}{\partial x} = i\beta$. So the curl equations again with respect to Figure 2.4 can be summed up as the following six scalar equations.

$$\frac{\partial H_y}{\partial z} = \omega\epsilon_0\epsilon E_x, \tag{2.14}$$

$$\frac{\partial H_x}{\partial z} - i\beta H_z = -i\omega\epsilon_0\epsilon E_y, \tag{2.15}$$

$$i\beta H_y = -i\omega\epsilon_0\epsilon E_z, \tag{2.16}$$

$$\frac{\partial E_y}{\partial z} = -i\omega\mu_0 H_x, \tag{2.17}$$

$$\frac{\partial E_x}{\partial z} - i\beta E_z = -i\omega\mu_0 H_y, \tag{2.18}$$

$$i\beta E_y = -i\omega\mu_0 H_z. \tag{2.19}$$

Transverse electromagnetic property of the waves could help at dealing with the equations given above. We can take the transverse magnetic (p polarized) and transverse electric (s polarized) modes into account separately. For TM mode we will have H_y, E_x and E_z components. Likewise, our nonzero components for TE mode are E_y, H_x and H_z. Consider the TE case first. Curl equations and the wave equation to be satisfied are,

$$H_x = i\frac{1}{\omega\mu_0}\frac{\partial E_y}{\partial z}, \tag{2.20}$$

$$H_z = \frac{\beta}{\omega\mu_0} E_y, \tag{2.21}$$

$$\frac{\partial^2 E_y}{\partial z^2} + (k_0^2\epsilon - \beta^2)E_y = 0. \tag{2.22}$$

Similar equations also hold for TM waves,

$$E_x = -i\frac{1}{\omega\epsilon_0\epsilon}\frac{\partial H_y}{\partial z}, \tag{2.23}$$

$$E_z = -\frac{\beta}{\omega\epsilon_0\epsilon} H_y, \tag{2.24}$$

$$\frac{\partial^2 H_y}{\partial z^2} + (k_0^2\epsilon - \beta^2)H_y = 0. \tag{2.25}$$

Having settled the basic equations, now we can investigate the boundary conditions that should hold at the metal insulator interface for surface plasmon propagation at a single metal layer case. Above we had stated that a wave, which is uniform at y-direction and propagating at an interface along x-axis is described as $\mathbf{E}(z)\mathrm{e}^{i\beta x}$. This equation is of course valid also for the $\mathbf{H}$ field. In our case, surface plasmons, the z-dependence is an exponential decay. So, if we consider a TM wave propagating at the interface, our equations for $z > 0$ are

$$H_y(z) = A_d \mathrm{e}^{i\beta x}\mathrm{e}^{-k_d z}, \tag{2.26}$$

$$E_x(z) = iA_d \frac{1}{\omega\epsilon_0\epsilon_d} k_d \mathrm{e}^{i\beta x}\mathrm{e}^{-k_d z}, \tag{2.27}$$

$$E_z(z) = -A_d \frac{\beta}{\omega\epsilon_0\epsilon_d} \mathrm{e}^{i\beta x}\mathrm{e}^{-k_d z}. \tag{2.28}$$

Similarly, for $z < 0$ we have,

$$H_y(z) = A_m \mathrm{e}^{i\beta x}\mathrm{e}^{k_m z}, \tag{2.29}$$

$$E_x(z) = -iA_m \frac{1}{\omega\epsilon_0\epsilon_m} k_m \mathrm{e}^{i\beta x}\mathrm{e}^{k_m z}, \tag{2.30}$$

$$E_z(z) = -A_m \frac{\beta}{\omega\epsilon_0\epsilon_m} \mathrm{e}^{i\beta x}\mathrm{e}^{k_m z}. \tag{2.31}$$

Continuity of H_y at the metal dielectric boundary requires that $A_m = A_d$. Similarly, we have a continuity requirement for $\epsilon_{m,d}E_z$ at the metal and dielectric layers respectively and this condition results to

$$\frac{k_d}{k_m} = -\frac{\epsilon_d}{\epsilon_m}. \tag{2.32}$$

This equation states that surface plasmons are sustained by the interfaces where the electric permittivities of the two layers have opposite signs, i.e. conductor-insulator interfaces. With respect to our metal-dielectric interface assumption this result does not seem surprising at all. We also know that H_y should satisfy Equation 2.25 for both $z < 0$ and $z > 0$.

$$k_d^2 = \beta^2 - k_0^2 \epsilon_d, \tag{2.33}$$

$$k_m^2 = \beta^2 - k_0^2 \epsilon_m. \tag{2.34}$$

Finally, when we introduce Equation 2.32 into Equations 2.33 and 2.34 we arrive to the dispersion relation of surface plasmons at a metal dielectric interface.

$$\beta = k_0 \sqrt{\frac{\epsilon_m \epsilon_d}{\epsilon_m + \epsilon_d}}. \tag{2.35}$$

Assuming that $\epsilon_m = \epsilon_m^{'} + i\epsilon_m^{''}$ and $|\epsilon_m^{'}| >> |\epsilon_m^{''}|$ we reach to

$$\beta = \beta^{'} + i\beta^{''} = k_0 \sqrt{\frac{\epsilon_m^{'} \epsilon_d}{\epsilon_m^{'} + \epsilon_d}} + i k_0 \frac{\epsilon_m^{''}}{2(\epsilon_m^{'})^2} \left(\frac{\epsilon_m^{'} \epsilon_d}{\epsilon_m^{'} + \epsilon_d} \right)^{3/2}. \tag{2.36}$$

where $\beta^{'}$ corresponds to the real wavevector of surface plasmons and $\beta^{''}$ represents the decay of SPPs propagating at the interface due to the loss at the metal.

We have derived surface plasmon dispersion relation for TM waves at a metal dielectric interface. Now, we should also investigate the TE modes whether we might obtain something interesting. TE modes for the same geometry are,

$$E_y(z) = A_d e^{i\beta x} e^{-k_d z}, \tag{2.37}$$

$$H_x(z) = -iA_d \frac{1}{\omega\mu_0} k_d e^{i\beta x} e^{-k_d z}, \tag{2.38}$$

$$H_z(z) = A_d \frac{\beta}{\omega\mu_0} e^{i\beta x} e^{-k_d z}. \tag{2.39}$$

for $z > 0$, and

$$E_y(z) = A_m e^{i\beta x} e^{k_m z}, \tag{2.40}$$

$$H_x(z) = -iA_m \frac{1}{\omega\mu_0} k_m e^{i\beta x} e^{k_m z}, \tag{2.41}$$

$$H_z(z) = -A_m \frac{\beta}{\omega\mu_0} e^{i\beta x} e^{k_m z}, \tag{2.42}$$

for $z < 0$. In this set of equations continuity of E_y at the interface again requires that $A_m = A_d$. Furthermore, we know that H_x is also continuous at the interface and this leads to

$$A_m(k_1 + k_2) = 0, \tag{2.43}$$

which is only satisfied for $A_m = A_d = 0$. Therefore, we conclude that surface plasmon modes occur only for TM waves. TE waves are not able to excite surface plasmons.

Dispersion relation given at Equation 2.35 and drawn at Figure 2.3 gives us significant information about behavior of SPPs. We have $Re(\epsilon_m) < 0$ and for realization of Equation 2.35 in real life we need real β' values. This requires

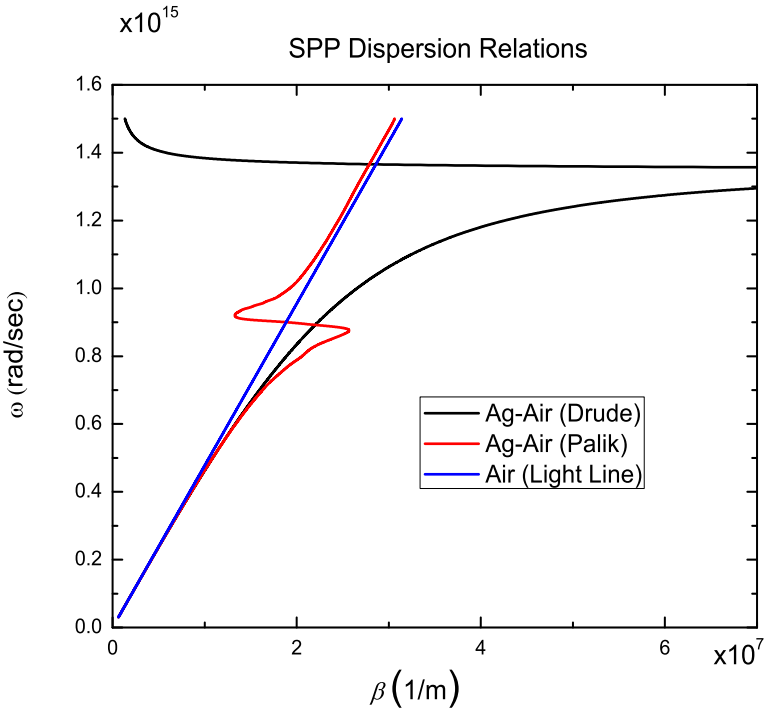

Figure 2.3: Dispersion relation for the surface plasmon polaritons on metal-dielectric interfaces.

that the expression in square-root needs to be positive. Thus, $\epsilon_m^{'} < -\epsilon_d$ and so is $\sqrt{\frac{\epsilon_m^{'}}{\epsilon_m^{'}+\epsilon_d}} > 1$. This final inequality mathematically proves that the wavevectors of surface plasmons at metal-dielectric interfaces are higher than the wave propagating at that dielectric. So it is not possible to directly couple light from air to a propagating SPP. The figure representing the dispersion of SPPs agrees with this statement as well. At this figure we see that defined β wavevectors for desired ω frequencies always lie below the light line which is the dispersion relation of electromagnetic waves at air. These curves do not have an intersection point where coupling of SPP could occur. Luckily, people developed some tricks, to increase the wavevector of incoming wave and excite surface plasmons at metal-air interfaces. In the following subsection we will discuss two of these methods that we used for our plasmonic structures.

2.2 SPP Coupling Techniques

2.2.1 ATR Prism Coupling

Prism coupling with usage of attenuated total reflection (ATR) is the most common method used for excitation of surface plasmons. The core idea is sending the light from a high index prism to the thin metal film. When light enters the prism its wavenumber becomes $k_p = k_0 n_p$. The light line of the prism, has an intersection point with the dispersion curve of surface plasmons on metal-air interface (figure not given here). This means, if we can satisfy the necessary conditions we can excite surface plasmons on metal-air interfaces with an optical wave sent through a prism. There are two main geometries available for this method, Kretschmann geometry [7] and Otto geometry [6].

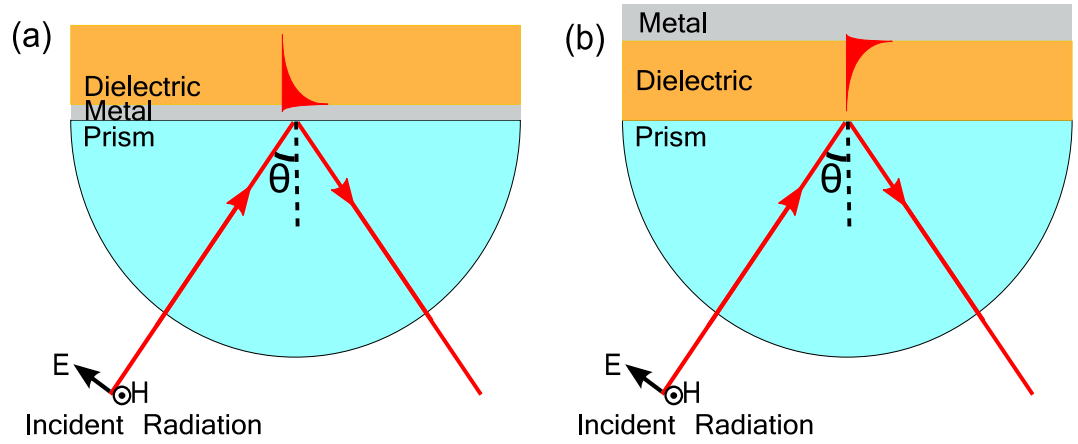

Figure 2.4: Different coupling geometries for prism coupling, Kretschmann **(a)** and Otto **(b)**

ATR part of this method is also worth mentioning. The incoming light is totally reflected from a prism metal interface for Kretschmann geometry or from a prism dielectric interface for Otto geometry. While it is being reflected it evanescently penetrates into the thin metal layer. This penetrated field oscillates free electrons of metal. If the interaction between the incident wave and electrons cause coherent oscillations of electrons, surface plasmon resonance condition occurs and the energy of the optical wave couples to surface plasmon waves

propagating at the metal dielectric interface. This transfer of energy is monitored as a dip at the reflection spectrum of incident wave.

The coupling condition for the geometry given at Figure2.4 is

$$k_0 n_p \sin\theta = k_{SPP} = k_0 \sqrt{\frac{\epsilon_m' \epsilon_d}{\epsilon_m' + \epsilon_d}} \tag{2.44}$$

which means that the horizontal momentum of the incident wave should match the momentum of the surface plasmon on metal-air interface. The spectrum of reflected light is given at Figure 2.5.

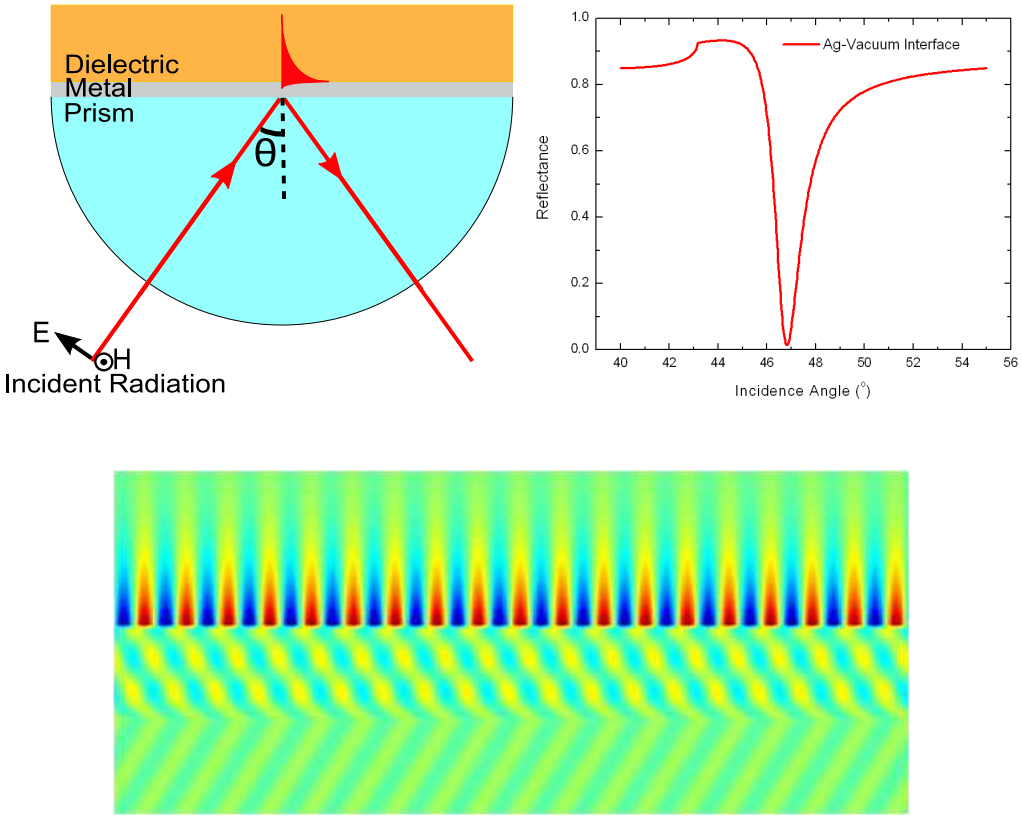

Figure 2.5: Typical prism coupling scheme. At the spectrum we see the resonance dip, at the field distribution we see the exponential behavior.

2.2.2 Grating Coupling

For the geometries, at which we do not have appropriate geometry to use prism coupling we use grating coupling instead. When an electromagnetic wave hits on

a grating which has a wavelength compatible with grating period it diffracts to different orders. Assume that we send a wave with wavevector k_0 at an incidence angle θ, horizontal wavevectors k_d of diffracted orders are

$$k_d = k_0 \sin\theta + m\frac{2\pi}{\Lambda} \tag{2.45}$$

where m is an integer denoting the diffraction order and Λ is the period of the grating. So, we see that we can increase the momentum of the incident wave using the gratings. This property brings up the idea of shining light from a dielectric directly onto a metal grating to excite surface plasmons at the dielectric metal interface. If the momentum of diffracted light can be tuned by changing the

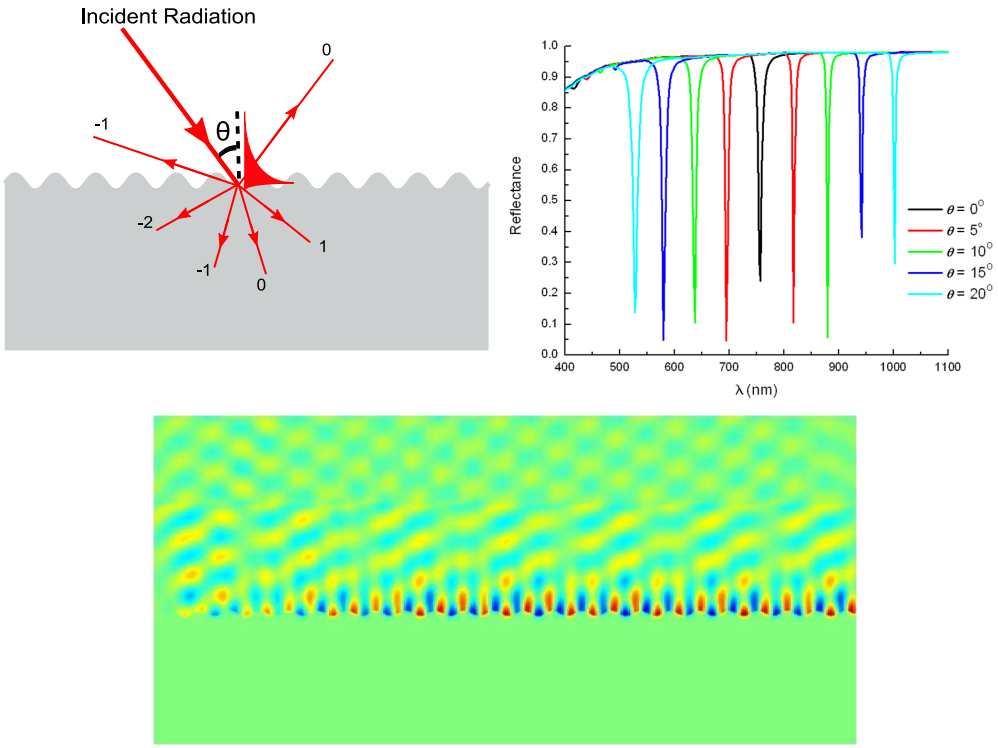

Figure 2.6: Typical grating coupling scheme. At the spectrum we see the resonance dips for different orders, at the field distribution we see the exponential behavior.

angle of incidence and wavelength of incoming light, resonance condition can be satisfied and surface plasmons are excited (Fig. 2.6). Therefore, surface plasmon coupling condition at a dielectric metal interface for grating coupling method is expressed as

$$\frac{2\pi}{\lambda} n_d \sin\theta + m\frac{2\pi}{\Lambda} = \frac{\omega}{c}\sqrt{\frac{\epsilon_m^{'}\epsilon_d}{\epsilon_m^{'} + \epsilon_d}} \tag{2.46}$$

$$n_d \sin\theta + m\frac{\lambda}{\Lambda} = \pm\sqrt{\frac{\epsilon_m^{'}\epsilon_d}{\epsilon_m^{'} + \epsilon_d}} \tag{2.47}$$

At the prism coupling case the propagation direction of the surface plasmon is same as the k_x wavevector direction of the incident wave. However, for grating coupling technique we have a number of diffracted orders and these orders can couple to surface plasmons propagating along forward or backward directions. This change in direction is represented with the $\pm$ sign at Equation 2.47. Oppositely propagating surface plasmons are shown as splitted resonance dips at the reflectance spectrum (Fig. 2.6).

Chapter 3

OPTICAL DISKS AS SPR TOOLS

In the previous parts we have given the historical and theoretical background of plasmonics. We also explained the methods to excite the surface plasmons. Now it is time for applications. To state again, highly remarkable properties of surface plasmons are subwavelength confinement of energy, highly sensitive resonance spectrum based on the change of refractive index and excitation of free electrons with optical waves. The mentioned properties make plasmonic devices appropriate for a variety of applications in sensing, optics and optoelectronics. Due to these potentials, plasmonics continues to draw attention and increasingly wider availability of high precision fabrication and characterization methods for submicron metallic structures allows further advances in the field of plasmonics. For the fabrication and utilization of plasmonic structures there are a number of methods, where certain geometric properties are dominant in determination of the conditions for resonant coupling.

In this chapter, we present the method we developed to convert optical disks (CD, DVD and Blu-Ray) into geometries optimal for study of high quality factor

grating coupled plasmon resonances (Fig. 3.1a-b). Previously, CDs and DVDs have been used in experiments involving grating coupled plasmons [24, 25]. However, to observe sharp resonances the depth and shape of corrugations must lie within a restricted range. A sharper resonance improves the overall sensitivity of plasmonic devices for biomolecular sensing. Moreover, high-Q resonances result in higher field enhancement factors which is important in a number of applications such as surface enhanced Raman scattering [26].

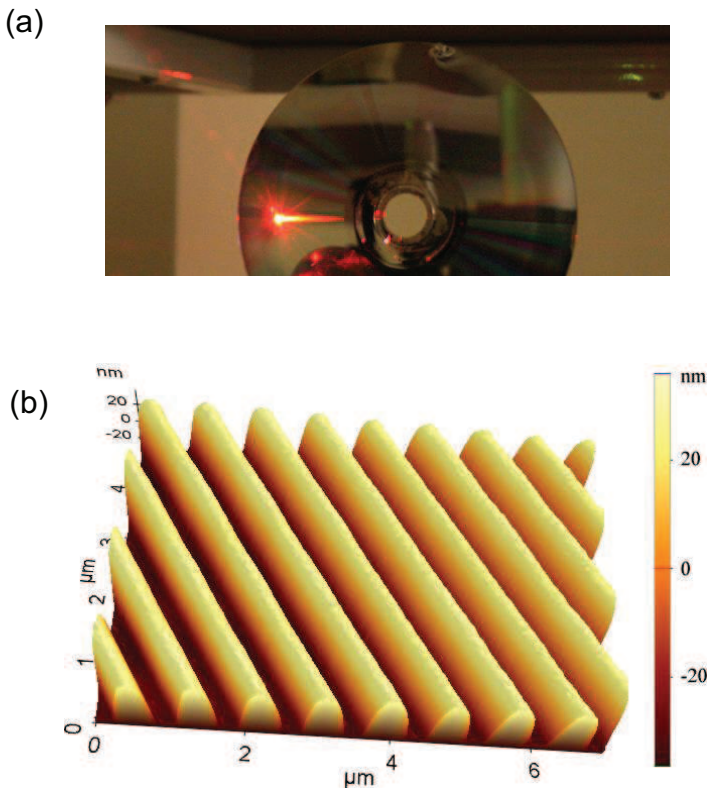

Figure 3.1: **(a)** Plasmonic excitation observed on a silver coated DVD surface. The observed coupling occurs at a single polarization and at a specific angle of incidence. **(b)** Surface topography by AFM shows the grating structure with a period $\Lambda = 740$ nm on the DVD.

From the methods described at the previous chapter we used grating coupling to excite surface plasmons on optical disks. This is a tricky but also an expectable method because most commercially available optical disks have corrugated imprinted surfaces protected by external coatings. All we need to do is to tune

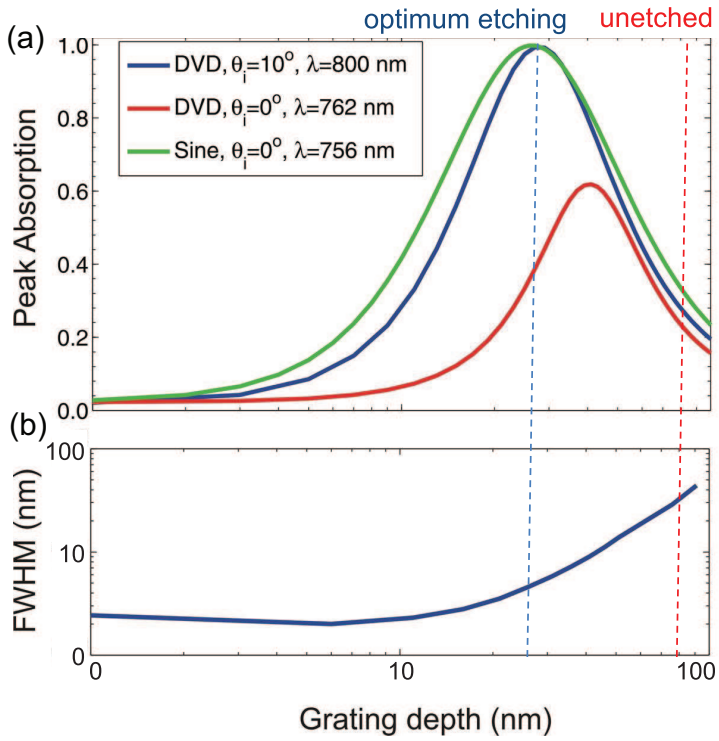

Figure 3.2: **(a)** Theoretical peak absorption due to grating coupled plasmon resonance on silver coated gratings on DVD with period $\Lambda = 740$nm at various angles of incidence as a function of grating depth and shape. Red curve shows a DVD that is not etched at an optimum level and it still has a rectangular type profile. Blue curve shows a DVD that is etched at an optimum level and converges to a sinusoidal grating (green curve). Peak absorption occurs at different wavelengths depending on the angle of incidence. **(b)** Full-width-at-half-maximum of the absorption peak for a grating with a DVD profile. Curves are calculated using rigorously coupled wave analysis.

these corrugations. By exposing the surfaces, simple chemical procedures can be used to tune the surface profile to optimal geometries for sharp and deep plasmon resonance peaks. The depth and shape of the grating affects the width (apparent quality factor) of the plasmon resonance. Also, the amplitude and relative phases of spatial Fourier components of the grating are important in determination of the reflection spectrum of such gratings [27, 28]. For higher peak absorption, which also means larger field enhancement due to stronger plasmon coupling, the factors that need to be tuned are the depth and shape of the gratings. In our case, we used rigorously coupled wave analysis (RCWA) to show the dependence

of peak absorption and quality factor on grating depth for sinusoidal grating profile and for a quasi-sinusoidal profile commonly observed in DVDs. Results of calculations are shown in Fig. 3.2a. It is seen that the peak absorption depends on the sinusoidality of the grating as well as the grating depth. For purely sinusoidal gratings, unity absorption is possible at normal incidence. For a grating with higher order harmonics (as is in a rectangular profile grating), the peak absorption may never reach unity for certain angles of incidence. Normal incidence of rectangular profile is shown in Fig. 3.2a where peak absorption can not exceed 0.65 due to coupling of different plasmon modes. However, as the angle is few degrees away from normal incidence, the absorption can still be close to unity for optimal grating depths, due to different dispersion of plasmon resonances associated with higher order harmonics and the fundamental harmonic. Also, presence of different spatial harmonics of the grating profile causes shifts in the peak wavelength as denoted in the legend of Fig. 3.2a. The width of resonances also depend on the grating depth as shown in Fig. 3.2b. Gratings with depths of 20 to 60 nm result in sharp resonances with full-width-at-half-maxima less than 10 nm. Unetched optical disk profiles (typically have 100 nm or more depth for CD and DVDs) are not optimal for observing sharp and strong resonances. In most applications it is desirable to have clean, sharp and strong resonances, the grating depths need to be reduced to an optimal depth and shapes must be made converged to a sinusoid.

3.1 Modification of optical disk profiles

Optical disks (CD, DVD and Blu-Ray) come in a wide variety of microscopic structures and use a wide range of materials. In this work, a relatively large number of disks (CD-R, CD-RW, DVD-R, DVD-RW, Blu-Ray recordable) from different manufacturers are studied. The rewritable disks (CD-RW and DVD-RW) generally use a hard chalcogenide material as the recording medium and

Blu-Ray write-once disks also use a multilayer hard coating. However, the write-once CD-R and DVD-R disks use a dye layer as the recording medium that can be dissolved in weaker solvents. Therefore, we focused on write-once disks for surface modification. Since different optical disk technologies have different layer structures, slightly different methods were used to prepare the grating substrates. CDs have a thin organic coating on top of a metal coating covering the dye layer and the grating, whereas the DVD-R structure consists of two polycarbonate disks with spiral grating surfaces in between. Blu-Ray disks have a relatively thin layer of transparent coating covering the grating layer. Towards the edges of the disks, the track spirals are well approximated by gratings with periods of Λ=1600 nm for the CD-R, Λ=740 nm for the DVD-R, and Λ=320 nm for Blu-Ray.

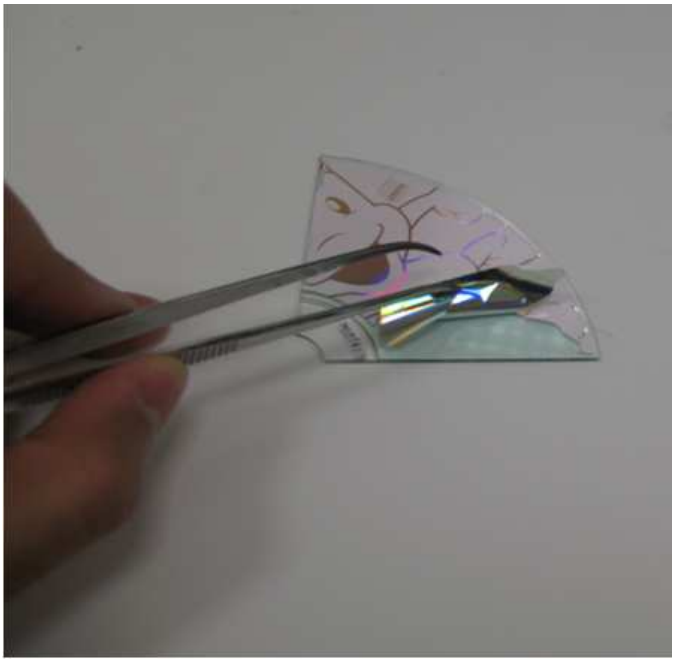

Figure 3.3: Peeling off procedure for top layer of a CD

For the case of the CD-R, the top protective layer was peeled off by exfoliation using a tape after delineation of the surface with a sharp cutter. After peeling off the top surface, the dye layer was removed by washing it with isopropanol. This procedure was observed not to change the corrugations on the disk but to

completely remove the dye. After cleaning, a 4:1 mixture of isopropanol and acetone was used to etch the grating to the desired depth. Typical etch times were found to be 10 seconds to few minutes. Slight agitation during etching was observed to be important for uniform and repeatable etching. Different brands of commercial CDs were used, and slight differences in corrugation depth and grating shape as well as differences in etch rates were observed. The surfaces are then coated with silver films of 50 to 100 nm thickness using thermal vacuum evaporation. In the case of DVD-R, due to the thick layers that protect the recording layer, instead of exfoliation by tape, the inner surface was exposed by first mechanically cutting a notch into the side of the disk and then by applying mechanical force to peel the two sides apart. Initial cut provides a location

Figure 3.4: Peeling apart procedure for separate layers of a DVD

for separation, which can be initiated from the side by a sharp cutter. The same procedure that was used for CD-R was also used for cleaning, etching and metal coating of DVD-R disks. Exposing the Blu-Ray disk gratings were done by peeling off the transparent thin coating by tweezers after cutting with

scissors. Unlike CD-R and DVD-R Blu-Ray disks have nearly sinusoidal grating shape with 20 nm grating depth which we don't need to modify and 320 nm grating period. This grating period brings plasmon resonances at around 320 nm wavelength depending on the angle of incidence. Since silver has enhanced absorption at this portion of the spectrum we used Al for metal coating of Blu-Ray.

3.2 Surface plasmons on tuned optical disks

The effect of etching on the topography of CD surfaces are measured using an AFM (PSIA XE100), as shown in Fig. 3.5a. It can be seen that unetched CD surfaces have grating profiles nearly rectangular with typical depths of 150 nm. Since the depth is important for the operation of the CD as an optical disk, different brand disks have similar corrugation depths. It is observed that, etching in acetone solution reduces the depth of the CD, as well as clearing the higher frequency components of the profile and changing it to a more sinusoidal shape. Depending on the choice ambient refractive index, angle of incidence and wavelength optimal depths for sharp and strong resonances will vary, and must be calculated. However, typical optimal depths for visible and near infrared wavelengths lay in the vicinity of 50 to 90 nm for the CDs. Therefore, 30 to 90 seconds of etching was found to be adequate.

The reflection spectra are measured using spectroscopic ellipsometry (J. A. Woollam, VASE) in the visible and infrared wavelengths as shown in Fig. 3.5b, where progressive appearance of sharp and strong plasmon resonance peaks can be observed in the reflection spectra. For an unetched substrate, variations in depth and width along the track lines and non-sinusoidal grating profiles cause broad and not-so-well defined resonances. However, as the surface is tuned by etching, sharper resonances appear in the reflection spectra. Also, measurements

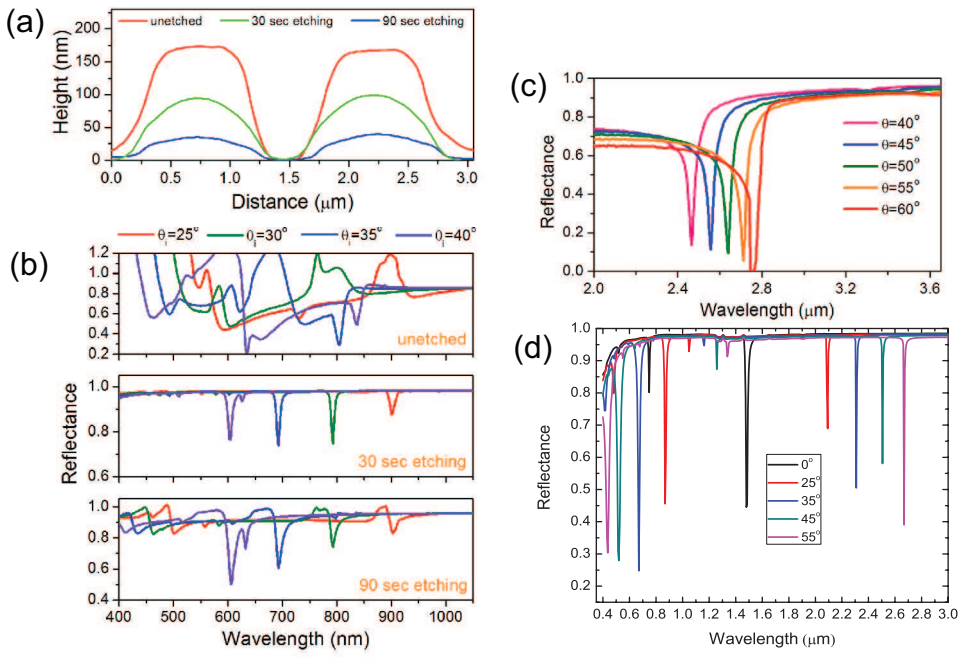

Figure 3.5: **(a)** Topographic profiles of the gratings on CD-R obtained by AFM for various etching time. **(b)** Reflection spectra as a function of wavelengths for various etching times measured on the CD-R disk coated with 50 nm Silver. **(c)** Grating coupled plasmon resonance at infrared region observed on CD surfaces coated with 50 nm of silver, at angles of incidence of 40, 45, 50, 55 and 60°. **(d)** Rigorously coupled wave analysis results for silver coated CD-R for angles of incidence 0, 20, 30 and 40°.

at different angles verify that the dips in the reflection spectra are due to grating coupled plasmon resonance. The plasmon resonances can also be observed in the infrared portion of the spectrum. An example of such resonances was observed using CDs, etched for 30 seconds and coated with a thin (50 nm) layer of silver. In this configuration, at angles of incidence of 40 to 60 degrees, plasmon resonances can be observed between 2.4 to 2.8 μm with quality factors of 54 to 30 (Fig. 3.5c). Figure 3.5d shows the calculated reflection spectra for various incidence angles by using rigorously coupled wave analysis. The results agree well with measurements at visible and infrared wavelengths.

For the DVDs, the etched profiles and corresponding reflection spectra are shown in Fig. 3.6a. The profiles of CDs and DVDs are different in shape. For most tested CDs, the unetched profiles show nearly symmetric rectangular profile,

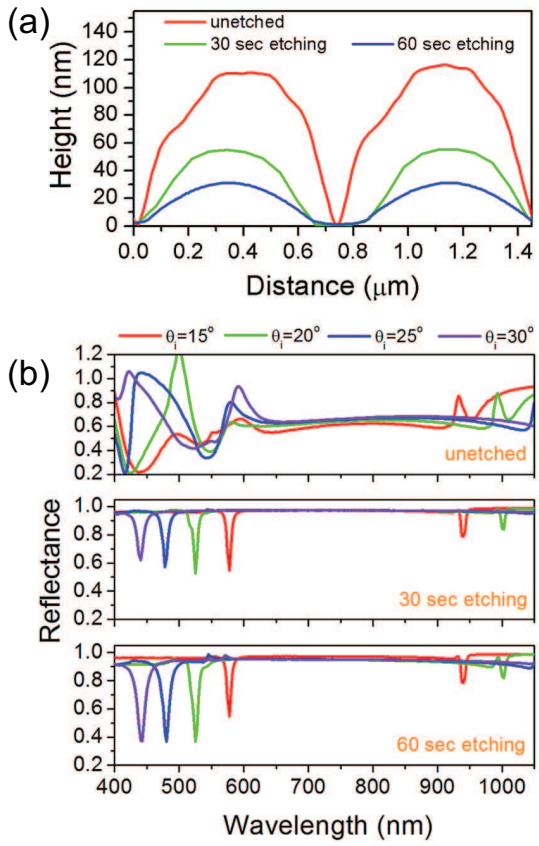

Figure 3.6: **(a)** Profiles of the gratings on a DVD-R disk obtained by AFM for various etching time. **(b)** The measured reflection spectra for various incidence angles on DVD-R disk coated with 50 nm Ag.

while the DVDs, have asymmetric profiles. Symmetric profile gratings as in CDs have odd spatial harmonics, whereas asymmetric profiles observed as in DVDs have both odd and even spatial harmonics. The relative intensities of harmonics change after etching, however, are partially preserved. Such harmonics are known to modify the plasmon band structure and can also lead to plasmonic band gaps [27]. It is possible to further control the grating shape in order to control relative intensities of spatial harmonics by using techniques such as evaporation of metal at an elevated angle.

The changes in the reflection spectra as a function of wavelength for various etch depths are shown in Fig. 3.6b. Similar to the CD, unetched DVDs show unclear resonances at all orders, while etching significantly improves apparent

quality factors of resonances. For example, the full width half maximum for 60 sec etched DVD substrates are from 5 nm to 25 nm for angles of incidence from 15 to 30 degrees. Again, experimentally observed angular dependence of the resonances agree well with the predictions of Equation 2.45.

Blu-Ray disks have significantly smaller periods than CDs and DVDs, and this makes them suitable for observing plasmon resonances at smaller wavelengths. The topographic profile and reflection spectrum as measured by spectroscopic ellipsometry is given in Fig. 3.7. Since the excitation wavelengths were near the UV for the Blu-Ray disks, aluminum was chosen as the metal layer. The

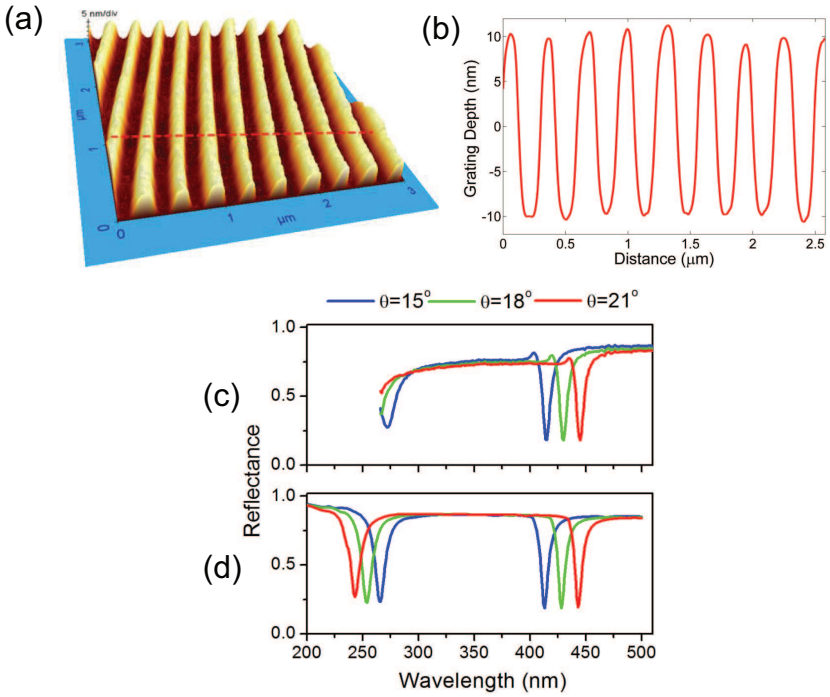

Figure 3.7: **(a)** AFM micrograph showing topography of Blu-Ray disk and **(b)** typical line profile. **(c)** Reflection spectra measured on a Blu-Ray disk coated with 50 nm Al at angles of incidence of 15, 18, and 21 degrees. **(d)** Calculated reflection spectra agree well with measured results.

so-called wobble patterns Fig. 3.7b along the grating lines limits the quality factors achievable with the untreated Blu-Ray disks, however small grating period

allows excitation of well defined resonances in the UV. Using Al coated Blu-Ray disks, plasmon resonances can be observed around 300 nm where DNA has resonant absorption (Fig. 3.7c). Even though measurements are incomplete due to limitation in the range of ellipsometer below 260 nm wavelengths, calculated results show distinct plasmonic absorption at UV region (Fig. 3.7d).

3.3 Observation of plasmon resonances in fluids

Once the disks are tuned for sharp resonances, many plasmonic effects and devices based on grating coupled plasmon resonance can be demonstrated. One of the most common applications of plasmon resonance is in biomolecular sensing. Such biosensors work by measuring the effective refractive index change due to molecular adsorption in an aqueous medium . Once functionalized for specific binding, the surfaces where the plasmon propagates can act as a biomolecular sensor [13, 14]. We demonstrate such a refractive index measurement setup in a simple fluid cell as shown in Fig. 3.8a. The shift of the plasmon resonance can be measured in the angular or wavelength interrogation modes. Using rigorously coupled wave analysis, reflection spectra of tuned DVD gratings in a fluid cell geometry can be simulated as is shown in Fig. 3.8b for water and isopropanol as fluid media for an angle of incidence 15°. The data shown in Fig. 3.8b shows shift of the plasmon resonance characterized by a spectroscopic ellipsometer for three different media, namely deionized water and isopropanol. It is seen that the data is in agreement with theoretical predictions. In the device configuration shown in Fig. 3.8a, the refractive index measurement can be performed in the angular interrogation scheme using a simple silicon photodiode and a simple laser diode. Although less sensitive compared to prisms in a wavelength interrogation type measurement [14], the advantage of the use of grating coupled plasmon resonance for biomolecular sensors is that high index substrates or prisms need not be used,

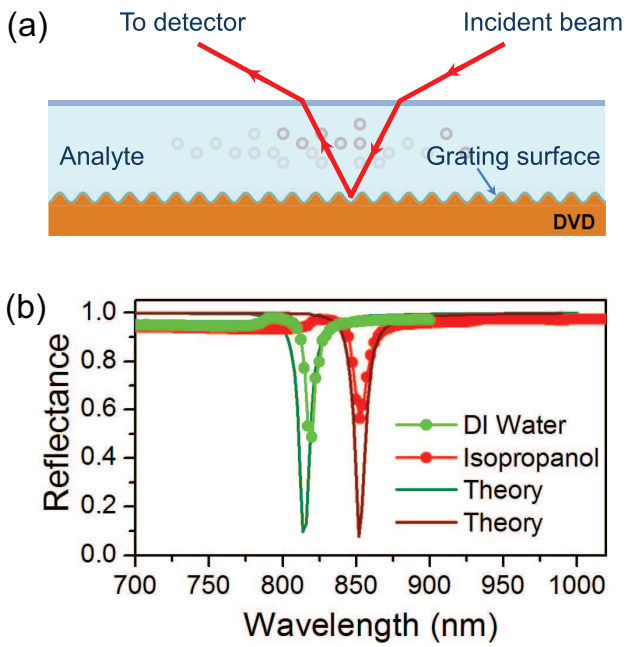

Figure 3.8: **(a)** Configuration used to observe grating coupled plasmon resonance in fluid. **(b)** Theoretical prediction and experimental data for the fluid being water and isopropanol.

and measurements can be performed at normal incidence. In this scheme, optical disks provide a disposable alternative for high sensitivity plasmon resonance biomolecular sensors.

Up to now we have shown how to modify optical disks by etching. Alternative procedures can also be used to modify the topography of optical disk gratings. Heat treatment (e.g. 150 °C , 5 minutes on a hotplate or 140 °C, 30 minutes in an oven) was observed to reflow the grating and produce extremely smooth sinusoidal gratings of about 30 nm depth, adequate for sharp GCPR lines. However, unless the disks are placed on flat substrates and unless they are heated and cooled slowly, flatness of the disks are compromised. As another alternative, oxygen plasma etching in a parallel plate PECVD system, was also observed to produce optimal corrugations without disturbing the disk flatness.

A pure sinusoidal metal coated grating has no spurious plasmon resonances and, the presented procedure does not produce perfectly sinusoidal surfaces. However, the tuned gratings are shown to behave like ideal sinusoidal gratings, for a wide range of incidence angles. The deviations from ideal sinusoids, can be observed in the reflection spectra. For example, the effect of wobble patterns and deviations from a pure sinusoid have been observed as a limitation in the peak absorption and widths of the resonances. Chemical etch tuning of the CD and DVDs were observed to reduce the effect of such secondary patterns. It was also observed that, a low surface roughness metal coating is important for observing higher quality factors. The surface roughness of silver layers can be increased by rapid metal evaporation. However, by reducing the evaporation rate or using sputter coating, smoother silver surfaces can be obtained, increasing the quality factors of resonances.

3.4 Demonstration of a Plasmonic Filter with Optical Discs

Although plasmonic structures have been extensively studied for better understanding of fundamental physical phenomenon, optoelectronic device applications generally focused on sensors. Since the pioneering works of Ebbesen [15] and Ghaemi [29] transmission of electromagnetic waves through thin metal films via plasmons has widely been studied. Plasmon resonance enhanced transmission through subwavelength holes, hole arrays or periodically corrugated metal surfaces have been investigated both theoretically and experimentally [30, 31, 32, 33]. The resonant transmission peaks due to interacting plasmonic structures (weak coupling regime) have been observed in Silver films containing an array of Silicon spheres [34]. Optical properties of the periodic

arrays of defects (voids) in mesoporous metals [35] and two-dimensional metallic quasi-photonic crystals [36] have also been investigated.

In this section we will explain how we could obtain plasmonic filters, that gives us sharp transmission peaks in coupled surface-plasmon on metallized grating structures. The grating structures are again obtained from optical storage disks. A filter based on plasmon enhanced transmission (PET) in metal coated coupled-grating structures is proposed and experimentally demonstrated. The filter consists of two metallized gratings placed back-to-back as shown in Fig. 3.9a. In an optimized layer structure with sufficiently thin metal layer, light is partially

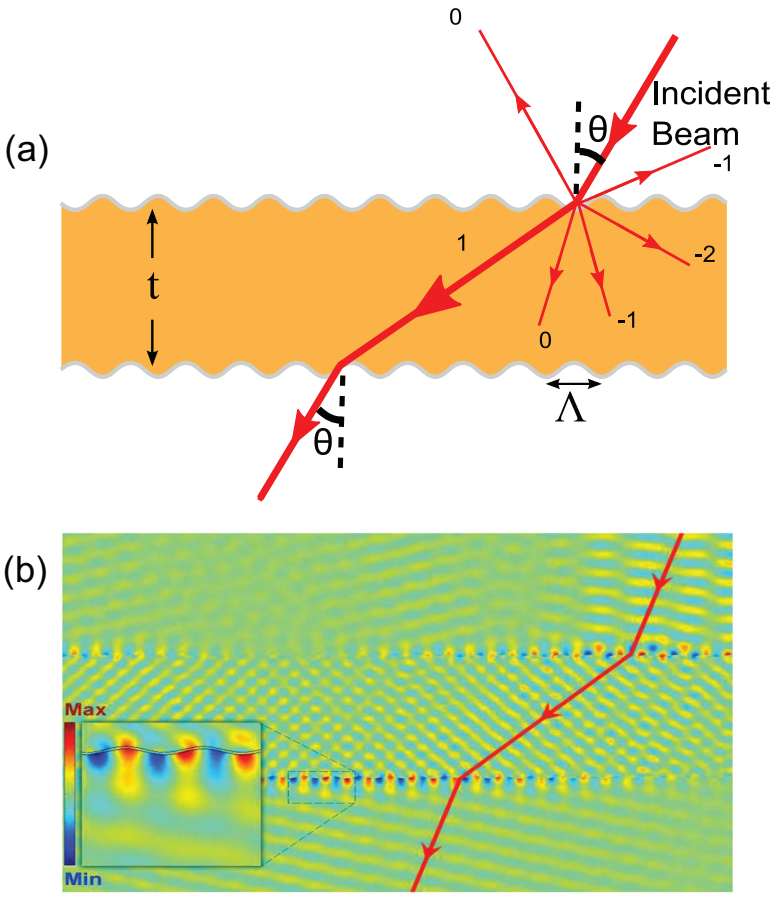

Figure 3.9: **(a)** Scheme of proposed filter structure. Top and bottom surfaces are parallel to each other. Both have the same grating period and silver coated on them is at the same thickness. **(b)** Calculated H field component of EM wave through coupled plasmonic structure agrees well with proposed scheme. Inset shows the plasmonic radiation from sinusoidal grating.

transmitted through the metal layer and is partially diffracted or re-emitted into different orders with different angles of propagation. For our proposed structure, the transmitted orders travel inside the substrate and are incident onto an identical grating on the other face of the substrate. Due to the symmetry of the device, components of the light wave that are generated through plasmonic emission recouple to the plasmon mode and a second event of plasmon enhanced transmission takes place at the second grating.

The distance between the two surfaces carrying the gratings, t, is very large compared to the plasmon propagation length and free space wavelength ($t \gg \xi$, λ). Under this condition, the reflected waves from the second surface do not interfere with (regenerate) the plasmons on the first surface, hence our analysis remains valid.

Figure 3.9b shows the calculated field distribution through the device for wavelength $\lambda = 580$ nm and angle of incidence $\theta_i = 15^\circ$ ($\Lambda = 740$ nm and $\Lambda \ll t$). It can be seen that the electromagnetic (EM) waves are re-emitted from second grating layer at the same angle of incidence as the incoming wave. Even though the dielectric layer thickness between the gratings is order of 1mm in real device structures, it is taken 10 μm to avoid computational difficulties in the finite difference time domain (FDTD) simulations. In this case, t is much larger than the wavelength of light of incident beam, but it is comparable to the plasmon propagation length.

Since our aim in this research is filter design, we first examined the transmission intensity through a single layer of silver-coated grating with $\Lambda = 740$ nm as a function of metal thickness (Fig. 3.10a) and wavelength (Fig. 3.10b) of incoming wave by using rigorously coupled wave analysis (RCWA).

As shown in Fig. 3.10a, the transmitted power for $+1^{\text{st}}$ diffraction order reaches its maximum value near 45 nm silver thickness for TM waves. On the

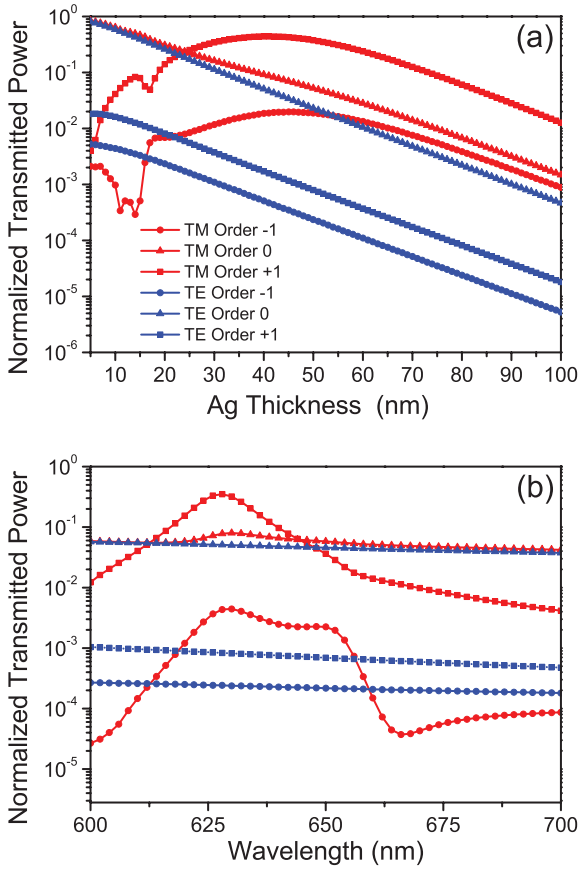

Figure 3.10: **(a)** Transmitted fraction of light on resonance as a function of metal thickness for incidence angle $\theta = 10°$ and $\lambda = 630$ nm. Since TE mode is not resonantly transmitted, the filter also acts as a polarizer, transmitting mainly TM polarization. Optimal Ag thickness is seen to be about 45 nm. **(b)** Transmitted fraction of light as a function of wavelength for the $-1^{st}, 0^{th}$ and $+1^{st}$ diffraction orders, for incidence angle $\theta = 10°$ and $t_{\mathrm{Ag}} = 45$ nm

other hand, the transmitted intensity for all the other diffracted orders for TE and TM waves are an order of magnitude smaller. Figure 3.10b shows wavelength dependence of transmitted power for different diffraction orders of both TE and TM modes. The maximum value of the $+1^{\mathrm{st}}$ diffraction order for TM mode for incidence angle $\theta_i = 10°$ occurs at wavelength $\lambda = 628$ nm. The filter acts also as a polarizer, with a TM/TE polarization ratio of about 100. This TM/TE ratio lets us think that this transmission might be due to the excited plasmon oscillations in the metal.

In order to implement our filter structure, we again used gratings present on optical storage disks. Surface modification of optical disks is again done with the same method described above. After this grating depth modification treatment two such surfaces are fixed back-to-back using a thin UV curable epoxy layer. Then the surfaces are metallized by vacuum evaporation of a 45 nm thick silver layer. A similar procedure was repeated using a CD, where the grating depth was tuned to 60 nm. The transmission through the structures were measured using spectrometric ellipsometers (J. A. Woollam VASE) in the visible and in the near infrared.

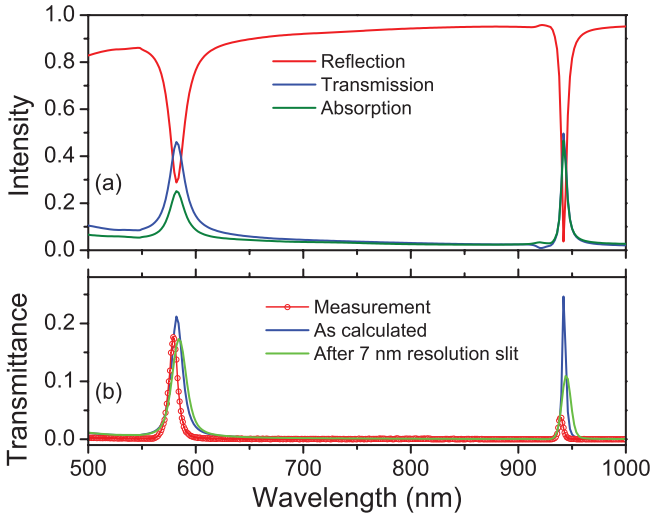

Figure 3.11: **(a)** Calculated reflection, transmission and absorption spectra as a function of wavelength for TM waves. Calculation parameters are grating period $\Lambda = 740$ nm, silver thickness $t_{\mathrm{Ag}} = 45$ nm and incidence angle $\theta = 15^{c}irc$. **(b)** Comparison of measured and calculated transmittance as a function of wavelength. Finite resolution of the spectrometer partially explains the discrepancy between calculations and measurement around 950 nm.

The total transmission through the coupled plasmonic grating structure as a function of wavelength for 15° angle of incidence is calculated by using RCWA and is shown in Fig. 3.11a, where $\Lambda = 740$ nm. The measured transmittance through the filter for $\theta_i = 15°$ shows peak at wavelengths $\lambda = 580$ nm and 940 nm. As shown in Fig. 3.11b, the simulations explain the measured spectra quantitatively if a finite spectrometer resolution is assumed.

Besides the theoretical prediction of transmittance we also performed FDTD simulations and experimentally measured the transmittance through the proposed plasmonic filter for various incidence angles ranging from $\theta_i = 0°$ to $20°$ (Fig. 3.12). It can be seen that, a peak transmission of up to 0.17 can be achieved

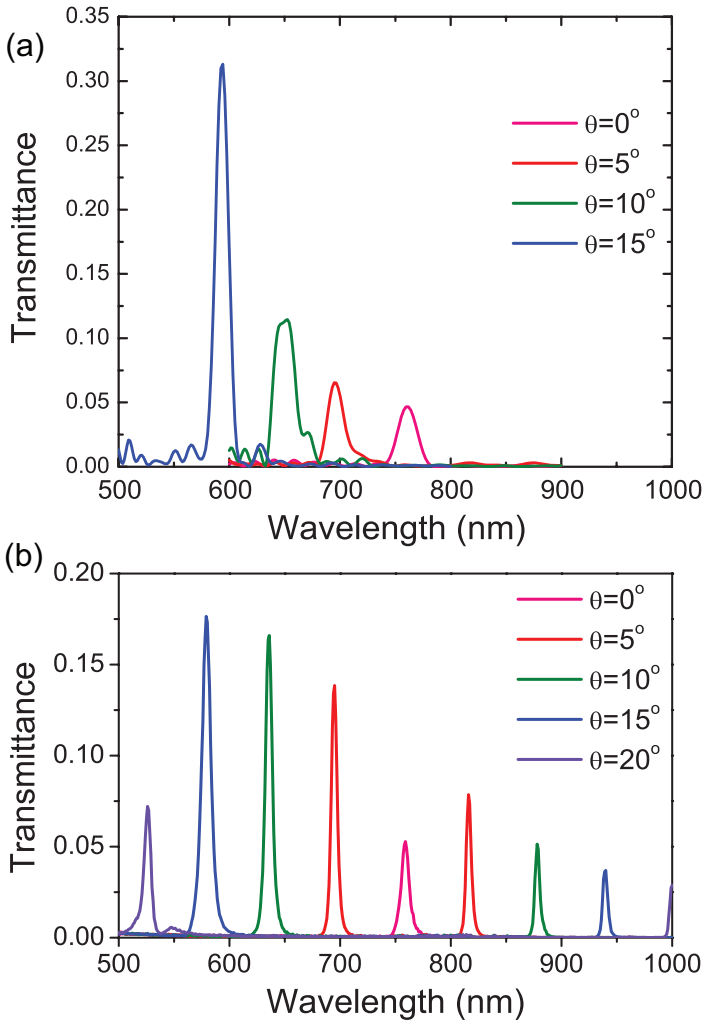

Figure 3.12: Transmitted intensity of a device having a grating period of $\Lambda = 740$ nm and t = 1 mm at various angles of incidence, as measured with a spectroscopic ellipsometer.**(a)** Simulation results, **(b)** Experimental measurements

experimentally over a broad wavelength range, with full width at half maximum (FWHM) of 10 to 5 nm. The positions of the experimental peaks agree well with the predictions of RCWA and FDTD simulations. For instance, the results shown at Fig. 3.2 predicts the transmission peak to occur at $\lambda = 628$ nm for 45 nm thick Ag coated grating and 10° of incidence angle, at the experiment

we obtain the transmission peak at $\lambda = 635$ nm for the same structure. At the FDTD simulations 0° simulations is exactly the same as the experimental measurements. However, when we move to higher angles we have a little deviation. This deviation is the result of boundary conditions set for FDTD. For 0° we used Bloch boundary conditions with only one period sample, when we increased the incident angle we moved on to periodic boundary conditions with larger samples.

For the device fabricated using CDs with grating periods of $\Lambda = 1600$ nm, plasmon enhanced transmission (PET) phenomenon can be observed in the near infrared portion of the spectrum at angles of incidence close to normal, as shown in Fig. 3.13. Due to finite transmission of the CD material (characterized by Fourier Transform Infrared (FTIR) spectrometer, data not shown), and relatively large thickness of the double CD substrate (3 mm), total transmission at

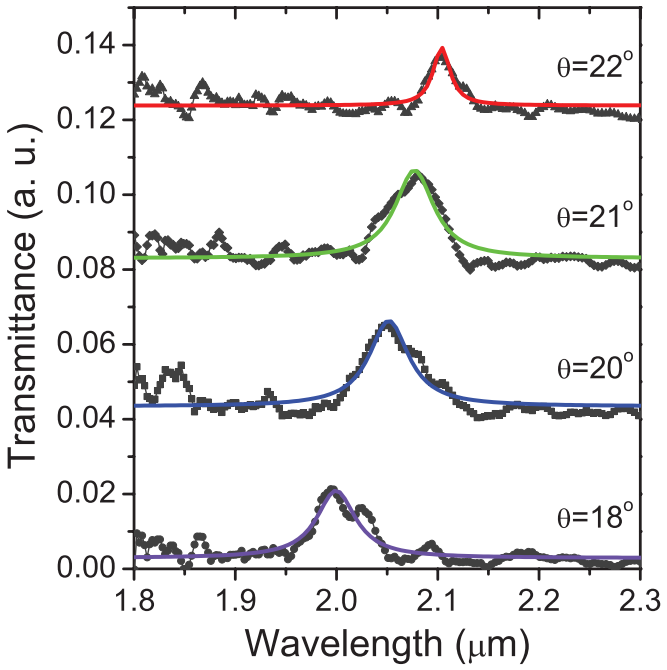

Figure 3.13: Measured transmitted intensity of a device having a grating period of $\Lambda = 1600$ nm (built on a CD) at various angles of incidence

the resonant wavelength is reduced to few percent. However, well defined resonances with widths of about 50 nm can be observed. This corresponds to a peak

wavelength to width ratio of about 40, which compares favorably with previously reported PETs at similar wavelengths.

In summary we proposed and demonstrated an optical filter that uses plasmon enhanced transmission through metallized gratings. The devices are realized using optical disks as starting substrates. Sharp transmission peaks with peak wavelengths dependent on the angle of incidence make the devices suitable for applications in compact spectrometers. By fabricating the device using an elastomeric substrate, peak wavelength can be tuned by applying strain. Theoretical calculations and measurements predict that such devices can be operated at infrared wavelengths by proper scaling. When used to filter collimated thermal emission, devices can be used to fabricate tunable, polarized infrared light sources, or disposable infrared spectrometers. It would be interesting to investigate an array of coupled plasmonic structures by varying the distance between plasmonic gratings.

Chapter 4

SURFACE PLASMONS AT MIM WAVEGUIDES

The work we will show at this chapter contains excitation of surface plasmons at metal-insulator-metal (MIM) systems. The question is, why should MIM plasmonic systems be an interesting research topic and what do we aim by that research?

4.1 An MIM Surface Plasmon Waveguide

From Chapter 2 we know that we have to have a resonance condition for excitation of surface plasmons. Again at Chapter 2 we saw that this resonance is observed as a single dip at the reflection spectrum. This single dip is the only mode of surface plasmon waveguide. Also from waveguide theory we know that if a system had more than one mode, each of these modes would correspond to a different field profile distribution at the system. Basing on the work of Bayindir [37], we presumed that if we perturb a stable system in some way and increase its modes from one to two, these two modes correspond to bonding and

anti-bonding modes of systems and the field profile observed becomes symmetric and anti-symmetric for each of these modes.

Final justification is why we need symmetric and anti-symmetric field distributions. By having such oppositely distributed field distributions we expected to obtain attractive and repulsive forces between metal layers. If we could calculate this force we would call it plasmonic force, but at this chapter we will just be concerned with excitation of these modes with numerical tools.

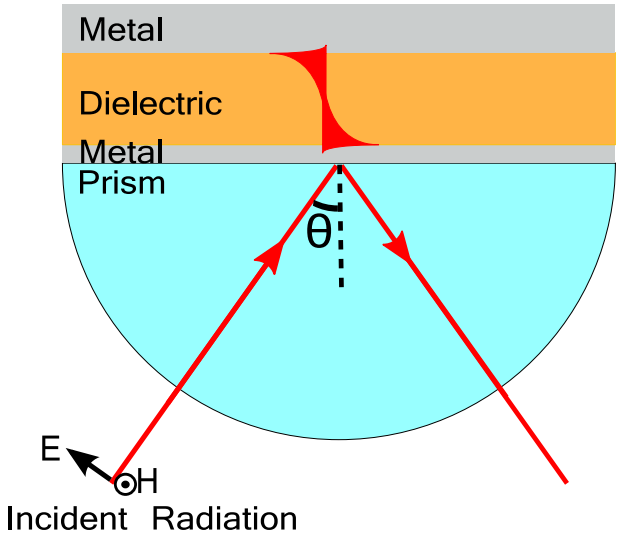

Figure 4.1: Coupling scheme to MIM surface plasmon waveguide from prism. TM wave is sent at incidence angle θ and the plasmon propagating at the first metal couples to the second metal.

We know that at a single layer metal(Ag,Au etc.) coated prism we have a metal insulator waveguide for the surface plasmon. From now on we consider the dielectric of dielectric-metal interface to be air. This surface plasmon is an inhomogeneous wave and it has a tail which is about one μm. This surface plasmon is excited on the metal air interface. If any material other than air enters to the one μm range this inhomogeneous wave will interact with that material and the stable waveguide system will be perturbed. Inspiring of this idea we assumed that we put a second silver interface 500 nm away from the first silver interface (Fig. 4.1). The idea is that the tail of surface plasmon will

penetrate into the second interface and it will oscillate the electrons of that silver coherently as well. From the interaction of two excited electron oscillations we might be able to excite more than one modes of the system.

For this system design we have some selection criteria. We took the prism material as SiO_2. We used silver as the metal due to its allowance for sharper resonances. Thickness of first silver layer is 50 nm due to plasmon excitation, second silver layer is taken as 300 nm thick. Why is the second layer thicker question may arise here. If we took second layer as 50 nm as well, surface plasmon wave penetrates all into the second metal and we get three modes excited (will be shown at the following subsections). That is why we select it 300 nm in our simulations. The 500 nm distance is predictably due to create a stronger interaction between the layers.

4.2 Theoretical Simulations

For the investigation of this system we used two approaches. One is simulation using Fresnel's multilayer reflection theory, second is FDTD method. At the Fresnel's equations part we used the formula for reflection at a single interface and we iteratively introduced it to multilayer reflection theory. Numerically speaking for a two layer system with respect to Figure 3.1 with dielectric constants ϵ_i and ϵ_j, wave numbers k_i and k_j which correspond to k_d and k_m with respect to Eqn 3.33 and Eqn 3.34

$$r_{ij} = \left(\frac{k_i}{\epsilon_i} - \frac{k_j}{\epsilon_j}\right) / \left(\frac{k_i}{\epsilon_i} + \frac{k_j}{\epsilon_j}\right) \tag{4.1}$$

This equation is valid if there is only one interface. For our case 4.2, due to the interference effects we should take the third layer into account as well. This gives us a reflection coefficient

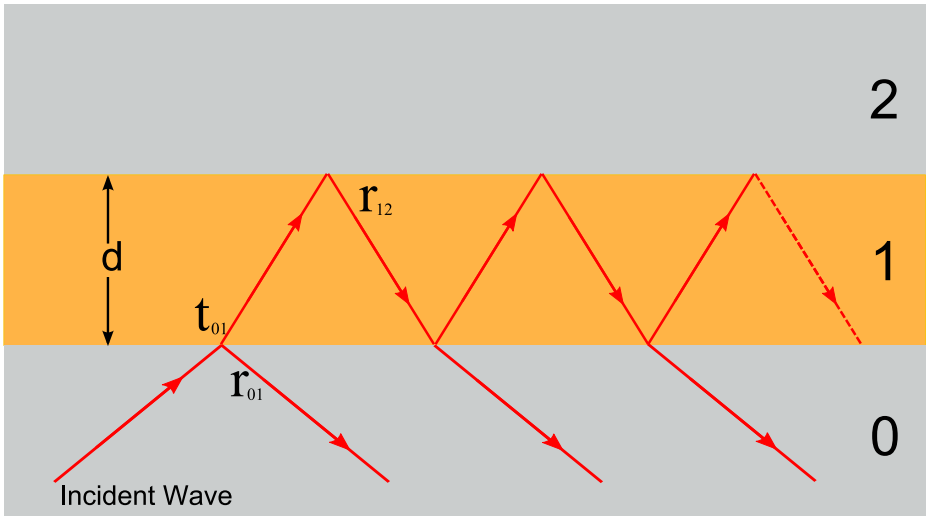

Figure 4.2: Fresnel coefficients for transmitted and reflected waves at the multi-layered material geometries. The numbers of materials are given as a reference to Equation4.2

$$r_{012} = \frac{r_{01} + r_{12}e^{2i\alpha}}{1 + r_{01}r_{12}e^{2i\alpha}} \tag{4.2}$$

with $\alpha = k_1 d_1$.

We coded these formulas in MATLAB and obtained our theoretical simulation results. For our simulations we started from the end, where we have infinite air, and iteratively came to the prism part. So we have become able to simulate multi layer structures without an upper limit e.g. IMI....MIM structures. A sample graph taken for MIM case is given at Figure 4.3. For the single layer Ag part we assumed 60 nm Ag coated on a prism with refractive index $n_p = 1.8$. The wavelength of the incident light is set to $\lambda = 500$ nm. With these circumstances we obtained the resonance at 36.1°. Then we have put one more Ag layer 700 nm away from the first layer and we got the second graph. At this figure we can clearly see that first stable mode is perturbed from new Ag and we can see the splitting at the spectrum.

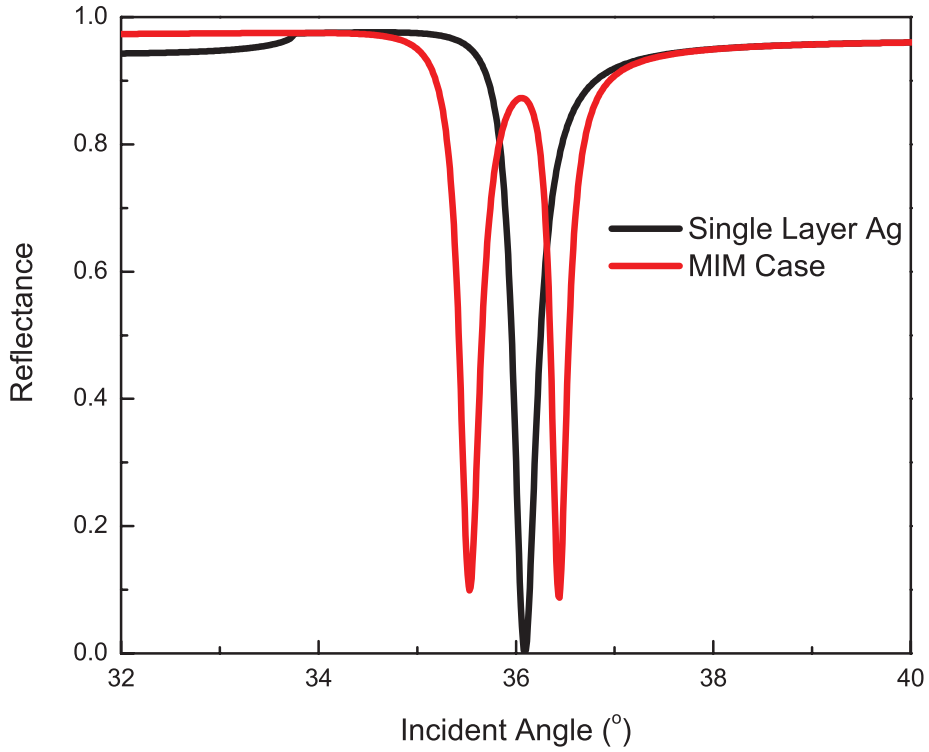

Figure 4.3: Observation of splitting phenomenon at theoretical simulations. Spectrum is scanned by changing incidence angle θ. Distance between layers d = 700 nm, wavelength $\lambda = 500$ nm and $n_p = 1.8$.

From this figure we can also deduce that the mode at the beginning is completely disappeared. If we were to send light again with incidence angle 36.1° we would get 80% reflectance i.e. non resonant situation.

A similar behavior is also seen at the frequency spectrum. While examining wavelength dependence we can also verify that this change at modes is due to perturbation. This is possible by looking at the spectrum change at different dielectric distances. At the simulation results given at Figure 4.4 we examined the dielectric thickness dependence from the wavelength spectrum perspective.

Incident angle for this simulation is set to $\theta = 43.6°$. When the system is not perturbed we have a single dip at 633 nm. When we bring second Ag layer closer we see the mode separation at about 1800 nm distance. When we shrink the distance we create a more powerful interaction between second metal and

the system. Due to this powerful interaction we see a wider separation of modes at the spectrum.

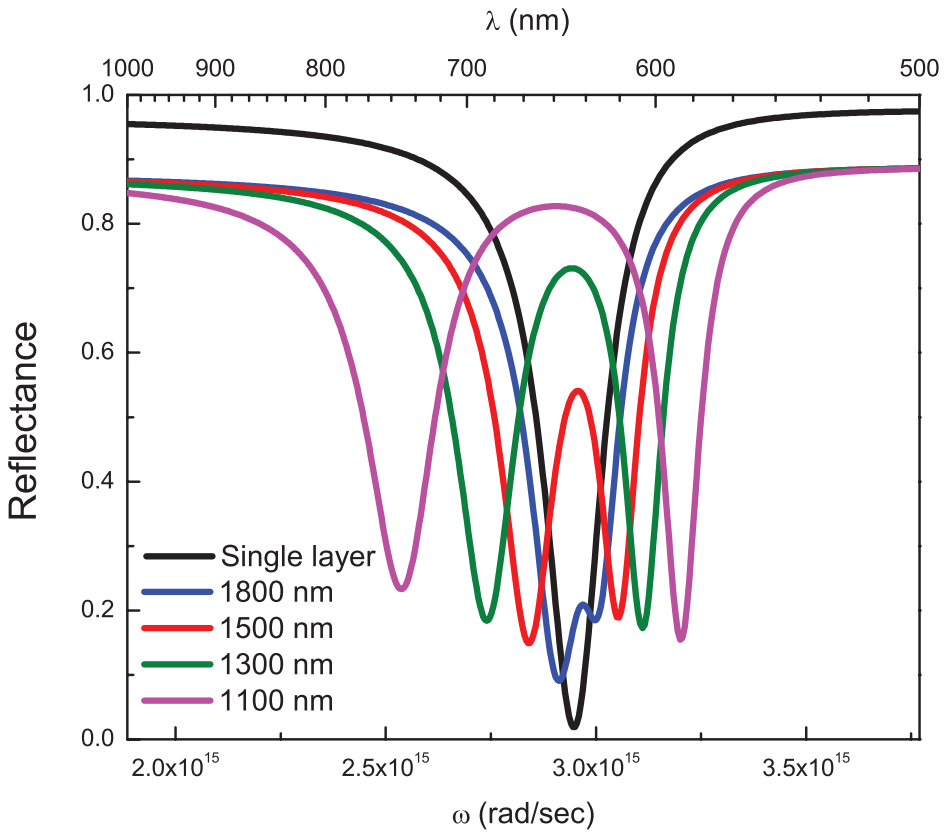

Figure 4.4: Effect of distance between layers, to splitting amount between the modes. As we see, while distance is decreasing, splitting at spectrum is increasing. This is what we expected due to stronger interaction at closer distances.

Now, it is also a good time to verify what we claimed about the thickness of the second metal. We said that for observing a more accurate splitting we had better use a thick (more that 200-300 nm) metal. We also claimed that if we used a thinner (50-100nm) metal as the second layer we would observe excitation of fundamental mode again at the system. The graph at Figure4.5 explains the situation better. At this figure the red curve shows the non-perturbed system. When we introduce a thick (200 nm) Ag metal to the system we observe the splitting (black curve) at the incident angle dependence. If we use a thin (70 nm) metal instead fundamental mode is again excited and this is not a case we would like. If we used even thinner metals (50 nm) the fundamental mode also

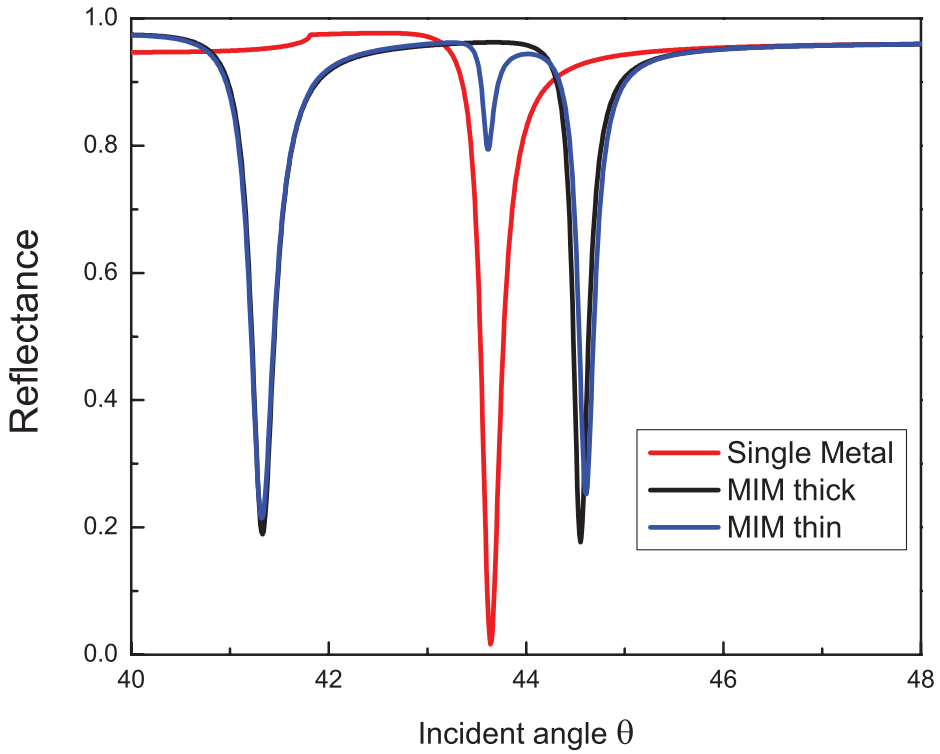

Figure 4.5: Observation of spectrum with respect to thickness of second metal layer. As we see when it is not thick enough it sustains two plasmon modes and one of them is the fundamental mode, and it perturbs the MIM splitting.

disturbs other modes' resonance angles. For that reason we preferred using thick metals.

4.3 FDTD Simulations

For the verification of what we theoretically presumed we need to show it experimentally. However, fabrication of the proposed device was not that easy. We have fabricated Ag bridge structures on a SiO_2 glass. Before fixing these glasses to the prism we etched the sacrificial layer to use air as the insulating material. At our etching trials we could not obtain an optimum MIM waveguide. Since the experiment way was partially closed we chose verification by FDTD simulations, which I call experimental simulations.

At this subsection I will give brief information and some results from our FDTD simulations for the proposed geometry. Our aim is to obtain the same spectrum with theoretical simulations and other than that observing the field distributions at the desired resonance regions. To do these both actions in an accurate and optimum way we searched for and tried a high number of FDTD programs. Finally we decided to use Lumerical Software which gives very good results at photonic spectrum.

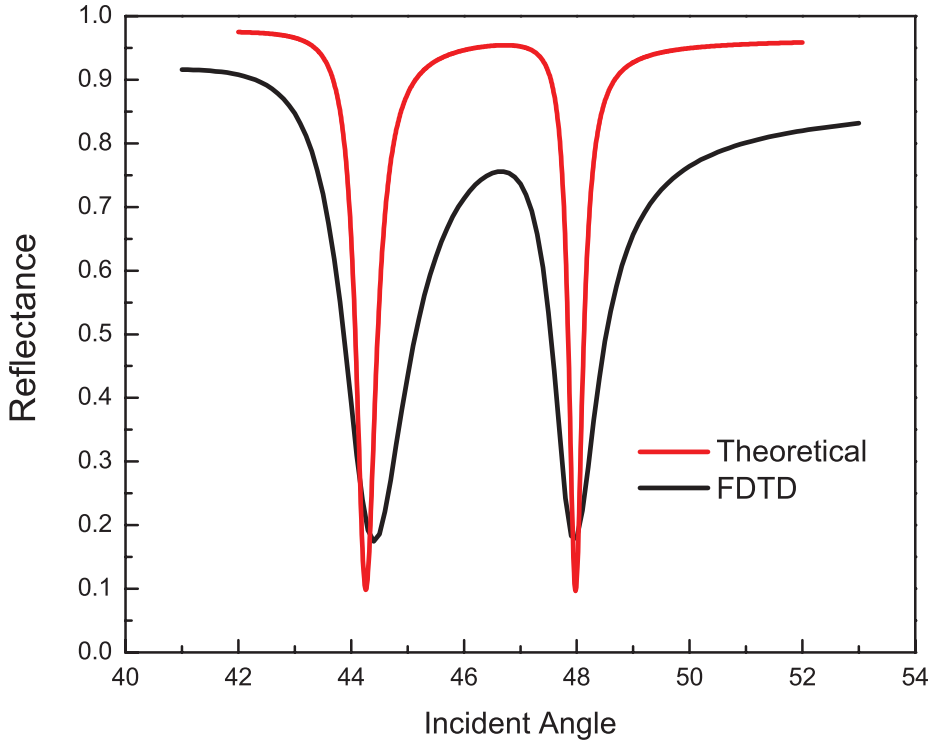

Figure 4.6: Comparison of theoretical simulations and FDTD simulations. The prism used at simulations is SiO_2. $n_p = 1.45$, $\lambda = 500$ nm, d = 500 nm. Both simulations are in good agreement with each other.

A typical spectrum comparison is as seen at Figure 4.6. This figure is the result of an incident wave at 500 nm wavelength, hitting to an MIM (Ag-air-Ag) with 500 nm distance in between the metals. At this figure we see some deviation between what we expected based on MATLAB results and what we obtained from FDTD simulations. This deviation look acceptable to us because theoretical simulations base on algebraic equations and give ideal results. On

the other hand, FDTD softwares divide the space into finite little areas and give an approximation to the experiment. And this approximation might create little deviations at both spectrum or intensity of electromagnetic waves.

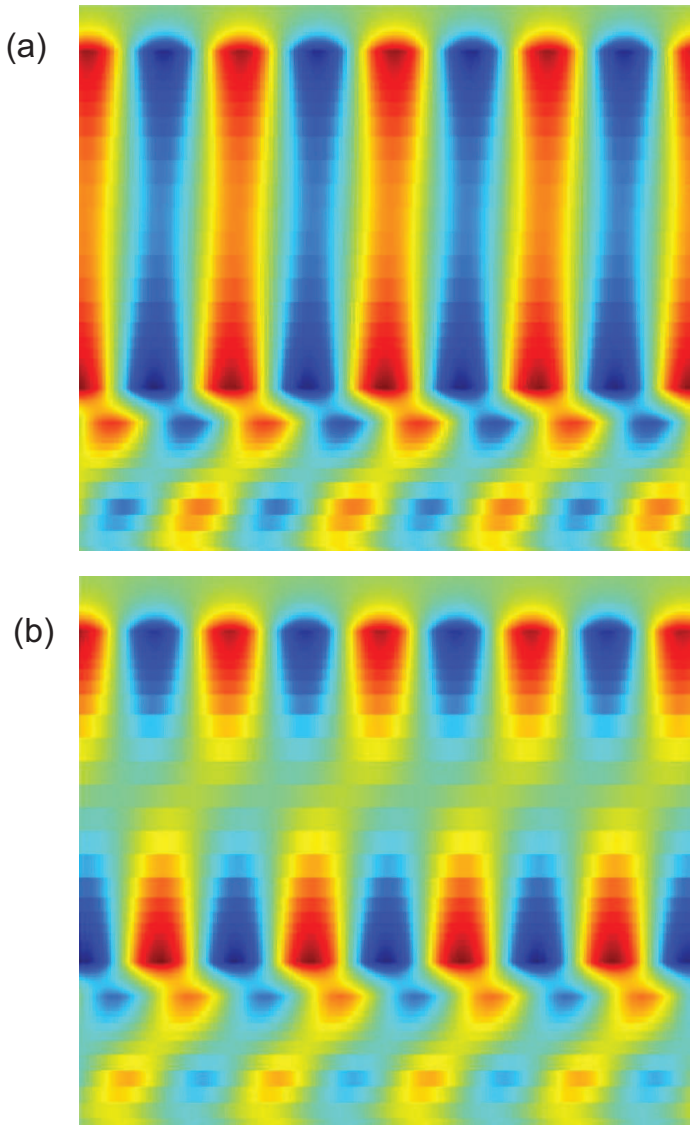

Figure 4.7: Field profile results of FDTD simulations. We observe the excited symmetric and anti-symmetric behaviors of surface plasmon waves clearly. **(a)** symmetric distribution at $\theta = 44.4°$ and **(b)** anti-symmetric distribution at $\theta = 47.95°$

On the other hand the important thing is that the spectral places of the resonance dips are very strongly correlated and there is very little deviation from

expected resonance wavelength. This result encourages us to examine the modes for possible symmetric and anti-symmetric field distributions. So we examine the field distributions at $\theta_1 = 44.4°$ and $\theta_2 = 47.95°$ separately. The results are shown at Figure 4.7

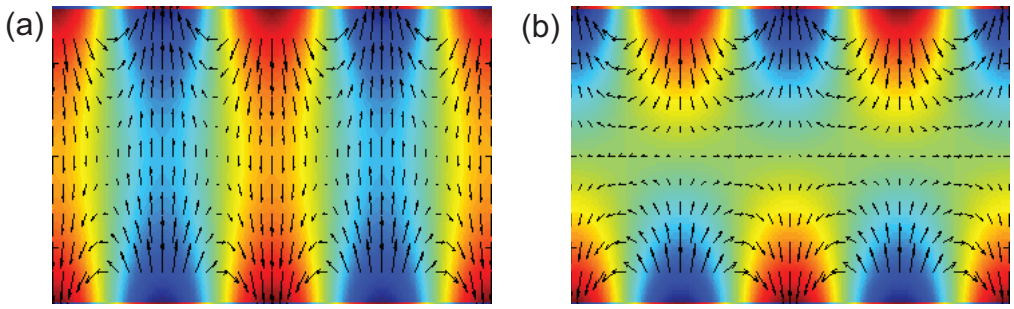

Figure 4.8: Electric field vectors for symmetric and anti-symmetric modes. Directions of these vectors give us information about excited force between layers. **(a)** symmetric mode, attractive **(b)** anti-symmetric mode, repulsive.

From the simulation results seen at Figure 4.7 these separated modes correspond to symmetric and anti-symmetric modes of the waveguide. The color represents the distribution of both H_z and E_x in algebraic size. Red shows positive and blue shows negative. The directions of the electric field for these modes are denoted by arrows and are shown in Figure 4.8. At the beginning we had said that all this work is done to calculate the plasmonic force. The idea of plasmonic force was based on these field lines. Electric field vectors are indicators of force directions. For the symmetric case (**(a)** part) we see that the field lines cause attractive force between layers. Similarly for the anti-symmetric case ((**(b)** part)) we get repelling force between the layers. The magnitudes of these forces can be calculated via different methods like Maxwell's stress tensor or from derivative of total energy. However, we left this subject at this point.

To conclude this chapter, we analyzed MIM surface plasmon waveguides. We theoretically and experimentally simulated the behavior of these waveguides. We saw that the stable single resonance spectrum changes when we bring a second metal closer to the system. Due to this perturbation we see a splitting type

behavior at the spectrum. When we have a closer look to these splitted modes we see that they are symmetric and anti-symmetric field distributions. These field distributions cause a force between the layers, calculation of which is left as future work.

Chapter 5

CONCLUSIONS

At this thesis we studied plasmonics at a number of different applications. First of all we used surface modified optical disks for excitation of surface plasmons. With this method we aimed to provide a compact working environment for plasmonics. We could realize grating coupling method efficiently, without using an interference lithography type fabrication procedure. We have shown how to etch the surfaces of optical disks and how this etching procedure affects the resonance quality. Since different disks have different grating periods we could achieve plasmon resonances at a wide spectrum ranging from UV to NIR.

Then we tried an application with this modified optical disks. At the simulations we have seen that light passes through thin layers of metal at resonance condition. This gave us inspiration to design a filter from these disks. We fabricated a device, with optimum gratings at both sides which are metal-coated. We verified our design with numerical simulations and experimental measurements. So we obtained an optical filter, the spectrum of which is wavelength, polarization and incident angle dependent. The transmission peaks of the filter could achieve quality factors as high as 100.

We finally worked on MIM waveguides for surface plasmons. At this part we examined the perturbation effect when we bring a metal close to a metal insulator waveguide. We observed a splitting at the spectrum due to perturbation. This splitting corresponded to bonding and antibonding modes of the system. So we expected to observe different field profiles at these separate modes and at the simulations we saw that these modes have symmetric and anti-symmetric field distributions respectively. Different field distributions suggest an excited force between metals, which we named plasmonic force.

Bibliography

[1] E. Hecht, *Optics*. Addison Wesley, San Francisco, 2003.

[2] R. D. Guenther, *Modern Optics*. John Wiley & Sons, New York, 1983.

[3] R. W. Wood, "On a remarkable case of uneven distribution of light in a diffraction grating spectrum," *Proc. Phys. Soc. London*, vol. 18, no. 1, pp. 269–275, 1902.

[4] U. Fano, "The theory of anomalous diffraction gratings and of quasi-stationary waves on metallic surfaces," *J. Opt. Soc. Am.*, vol. 31, pp. 213–222, 1941.

[5] T. Turbadar, "Complete absorption of light by thin metal films," *Proc. Phys. Soc.*, vol. 73, pp. 40–44, 1959.

[6] A. Otto, "Towards multimaterial multifunctional fibres that see, hear, sense and communicate," *Zeitschrift für Physik*, vol. 216, pp. 398–410, 1968.

[7] E. Kretschmann and H. Raether, "Dynamic all-optical tuning of transverse resonantcavity modes in photonic bandgap fibers," *Z Naturforschung*, vol. 23a, p. 2135, 1968.

[8] W. L. Barnes, A. Dereux, and T. W. Ebbesen, "Surface plasmon subwavelength optics," *Nature*, vol. 424, pp. 824–830, 2003.

[9] E. Ozbay, "Plasmonics: Merging photonics and electronics at nanoscale dimensions," *Science*, vol. 311, pp. 189–193, 2006.

[10] H. Atwater, "Promise of plasmonics," *Scientific American*, pp. 56–63, April 2009.

[11] J. C. Quail, J. G. Rako, H. J. Simonand, and R. T. Deck, "Optical second-harmonic generation with long-range surface plasmons," *Phys. Rev. Lett.*, vol. 50, pp. 1987–1989, 1983.

[12] N. C. Panoiu and R. M. Osgood, "Subwavelength nonlinear plasmonic nanowire," *Nano Lett.*, vol. 4, pp. 2427–2430, 2004.

[13] J. Homola, "Surface plasmon resonance sensors for detection of chemical and biological species," *Chem. Rev.*, vol. 108, pp. 462–493, 2008.

[14] J. Homola, S. S. Yee, and G. Gauglitz, "Surface plasmon resonance sensors: review," *Sensors and Actuators B*, vol. 54, pp. 3–15, 1999.

[15] T. W. Ebbesen, H. J. Lezec, H. F. Ghaemi, T. Thio, and P. A. Wolff, "Extraordinary optical transmission through sub-wavelength hole arrays," *Nature*, vol. 391, pp. 667–669, 1998.

[16] J. A. Dionne, L. A. Sweatlock, H. A. Atwater, and A. Polman, "Plasmon slot waveguides: Towards chip-scale propagation with subwavelength-scale localization," *Phys. Rev. B*, vol. 73, pp. 035407(1)–035407(9), 2006.

[17] H. T. Miyazaki, "Squeezing visible lightwaves into a 3-nm-thick and 55-nm-long plasmon cavity," *Phys. Rev. Lett.*, vol. 96, pp. 097401(1)–097401(4), 2006.

[18] T. Kurokawa and H. T. Miyazaki, "Metal-insulator-metal plasmon nanocavities: Analysis of optical properties," *Phys. Rev. B*, vol. 75, pp. 035411(1)–035411(13), 2007.

[19] B. Kaplan, H. Guner, O. Senlik, K. Gurel, M. Bayindir, and A. Dana, "Tuning optical disks for plasmonic applications," *Plasmonics*, 2009.

[20] K. Gurel, B. Kaplan, H. Guner, M. Bayindir, and A. Dana, "Resonant transmission of light through surface plasmon structures," *Applied Physics Letters*, vol. 94, p. 233102, 2009.

[21] P. Drude, "Zur elektronentheorie der metalle.," *Ann. Phys.*, vol. 1, pp. 566–613, 1900.

[22] P. B. Johnson and R. W. Christy, "Optical constants of the noble metals.," *Phys. Rev. B*, vol. 6, pp. 4370–4379, 1972.

[23] S. A. Maier, *Plasmonics Fundamentals and Applications*. Springer, 2007.

[24] E. Fontana, "Theoretical and ecperimental study of the surface plasmon resonance on a recordable compact disk," *Appl Opt*, vol. 43, pp. 79–87, 2004.

[25] N. Sedoglavich, R. Kunnemeyer, S. R. Dalele, and J. Sharpe, "Phase-polarization contrast for surface plasmon resonance based on low cost grating substrates," *Current Applied Physics*, vol. 8, pp. 351–354, 2008.

[26] K. Kneipp, H. Kneipp, I. Itzkan, R. R. Dasari, and M. S. Feld, "Surface enhanced raman scattering and biophysics.," *J Phys Chem*, vol. 14, pp. 597–624, 2002.

[27] A. Kocabas, G. Ertas, S. S. Senlik, and A. Aydinli, "Plasmonic band gap structures for surface-enhanced raman scattering," *Opt Express*, vol. 16, pp. 12469–12477, 2008.

[28] A. Kocabas, S. S. Senlik, and A. Aydinli, "Plasmonic band gap cavities on biharmonic gratings," *Phys Rev B*, vol. 77, no. 19, pp. 195130(1)–195130(7), 2008.

[29] F. Ghaemi, T. Thio, D. E. Grupp, T. W. Ebbesen, and H. J. Lezec, "Surface plasmons enhance optical transmission through subwavelength holes," *Phys Rev B*, vol. 58, p. 6779, 1998.

[30] I. Avrutsky, Y. Zhao, and V. Kochergin, "Surface-plasmon-assisted resonant tunneling of light through a periodically corrugated thin metal film," *Opt Lett*, vol. 25, pp. 595–597, 2000.

[31] N. Bonod, S. Enoch, L. Li, E. Popov, and M. Nevière, "Resonant optical transmission through thin metallic films with and without holes," *Opt Express*, vol. 11, pp. 482–490, 2003.

[32] Y.-H. Ye and J.-Y. Zhang, "Enhanced light transmission through cascaded metal films perforated with periodic hole arrays," *Opt Lett*, vol. 30, pp. 1521–1523, 2005.

[33] H. E. Went, A. P. Hibbins, J. R. Sambles, C. R. Lawrence, and A. P. Crick, "Selective transmission through very deep zero-order metallic gratings at microwave frequencies," *App Phys Lett*, vol. 77, p. 2789, 2000.

[34] F. J. G. de Abajo, G. Gómez-Santos, L. A. Blanco, A. G. Borisov, and S. V. Shabanov, "Tunneling mechanism of light transmission through metallic films," *Phys Rev Lett*, vol. 95, p. 067403, 2005.

[35] N. Stefanou, A. Modinos, and V. Yannopapas, "Optical transparency of mesoporous metals," *Solid State Commun.*, vol. 118, p. 69, 2001.

[36] M. Bayindir, E. Cubukcu, I. Bulu, and E. Ozbay *Europhys. Lett.*, vol. 56, p. 41, 2001.

[37] M. Bayindir, B. Temelkuran, and E. Ozbay, "Tight-binding description of the coupled defect modes in three-dimensional photonic crystals," *Phys Rev B*, vol. 84, pp. 2140–2143, 2000.